Geometric perspective for explaining Hubble tension: theoretical and observational aspects

OPEN ACCESS
IOP Publishing
Classical and Quantum Gravity
Class. Quantum Grav. **40** (2023) 195006 (29pp)
https://doi.org/10.1088/1361-6382/aceacc

Geometric perspective for explaining Hubble tension: theoretical and observational aspects

Robert Monjo[1,*] **and Rutwig Campoamor-Stursberg**[2]

[1] Department of Algebra, Geometry and Topology, Complutense University of Madrid, Plaza de las Ciencias 3, E-28040 Madrid, Spain
[2] Instituto de Matemática Interdisciplinar (IMI), Universidad Complutense de Madrid, Plaza de las Ciencias 3, E-28040 Madrid, Spain

E-mail: rmonjo@ucm.es

Received 4 April 2023; revised 11 June 2023
Accepted for publication 26 July 2023
Published 30 August 2023

Abstract

The Universe expansion rate has two different but very precise values (67.4 ± 0.5 and 73.30 ± 1.04 km s^{-1}Mpc^{-1}) that are not compatible. This problem, known as a Hubble tension, adds to other cosmological questions such as the origin of dark energy and the flatness problem. In turn, alternative models have attempted to explain similar phenomena but without dark energy. The aim of this work was to explain the Hubble tension by using a geometrical interpretation of observational viewpoints in embedded manifolds. Our technique consists of a set of parametric projections of radially inhomogeneous metrics, linking indistinguishable behaviours of accelerated flat and non-accelerated closed universes. A dark-energy-like phenomenon emerges from the distortion of matter-independent hyperconical metrics. To contrast our model, numerical solutions of dark energy/matter densities and Hubble parameter were obtained and compared to the standard model fitted to the Pantheon Supernovae Ia sample and in contrast to the SH0ES LMC Cepheid findings. Finally, Hubble tension is modelled by the different extrinsic/intrinsic viewpoints of the manifold. Compared to the Planck Legacy's 2018 release of $H_0 = 67.4 \pm 0.5$ km s^{-1}Mpc^{-1}, we found ΛCDM-dependent

* Author to whom any correspondence should be addressed.

(intrinsic) ranges between 66.38 and 68.87 km $s^{-1}Mpc^{-1}$, which were theoretically derived by setting local compatibility of metrics. The ΛCDM-independent extrinsic viewpoint resulted in a Hubble parameter between 73 and 74 km $s^{-1}Mpc^{-1}$ (compared to $H_0 = 73.30 \pm 1.04$ km $s^{-1}Mpc^{-1}$ of SH0ES). Datasets of 1048 Pantheon Type Ia supernovae ($0.0101 < z < 2.26$) and 34 cosmic chronometers combined with 7 radial baryon acoustic oscillation size-based samples ($0.0708 < z < 1.965$) were used to constraint the model. According to this geometrical perspective, dark parameters (energy and matter) could partially or totally be considered 'apparent physical quantities', a consequence of the stereographic projection of the extrinsic curvature.

Keywords: dark energy, dark matter, cosmological parameters, Hubble parameter

(Some figures may appear in colour only in the online journal)

1. Introduction

1.1. Two different dynamics?

'Hubble tension' is a term commonly used in cosmology to refer to the discrepancy between different measurements of the Hubble constant (H_0). For instance, the Cepheid Supernovae (SNe) sample leads to $H_0 = (73.3 \pm 1.04)$ km $s^{-1}Mpc^{-1}$ when SH0ES uses 'cosmic distance ladder' [1, 2, 3], while Planck Legacy 2018 (PL18) found it to be $H_0 = (67.4 \pm 0.5)$ km $s^{-1}Mpc^{-1}$ [4] by analysing data from the cosmic microwave background (CMB). In an extensive review [5], proposals to resolve the Hubble tension were classified in the following categories: dark energy models, inflationary models and modified gravity among others. Particularly, modified gravity and cosmological models with (extra) non-gravitational interactions have successfully alleviated the H_0 tension, but they cannot be simultaneously adjusted to baryon acoustic oscillation (BAO) and SNe Ia data [5]. Radially inhomogeneous universes can locally reduce the Hubble tension [6, 7]. For example, the inclusion of curvature-mass profiles in the Lemaître–Tolman–Bondi (LTB) metric (ΛLTB) produces similar effects to the standard ΛCDM, with a tension reduction for $0.023 < z < 0.15$ [7]. Spatial inhomogeneities can be angular (like LTB) or only radial (like the Hyperconical model), with a different luminosity-angular distance relation [6]. On the other hand, as an 'inhomogeneity in the time', a new constraint on Early Dark Energy was recently proposed to solve the problem [8–10]. Applying this method to the Planck and BOSS data, $H_0 = 69.52^{+0.95}_{-1.21}$ km s^{-1} Mpc^{-1} is obtained, which only partially alleviates the Hubble tension [11].

The difference between local and global geometry could play a role in determining the origin of the Hubble tension. An example of this is given in [12], which hypothesised that the local Hubble flow is due to the repulsive dark-energy term in the weak-field limit of Einstein's filed equations. Within this idea, two different perspectives (globally relativistic and locally non-relativistic cosmologies) provide values for the lower and upper constraints of the Hubble parameter: $\sqrt{\Lambda c^2/3} \approx 56.2$ and $\sqrt{\Lambda c^2} \approx 97.3$ km $s^{-1}Mpc^{-1}$.

Observational Hubble parameter data, mainly cosmic chronometers (CCs) and radial BAO size-based methods, can aid in the exploration of time evolution and the scale differences of cosmological parameters [13]. For instance, the CC method proposed by Jimenez and

Loeb [14] uses relative galaxy ages to estimate the Hubble parameter, which has been widely considered to directly measure the expansion of the Universe at different redshift scales [15, 16]. Instead, BAO data constraint combines the 'sound horizon scale' and the Hubble parameter. Thus, extra data is required to calibrate the size of the sound horizon (usually CMB anisotropy measurements or Lyα forest) and, with this, constrain the Hubble parameter [17]. Galaxy redshift surveys also provide estimations on cosmological parameters by combining to radial BAO lengths. It allows the extraction of (unbiased) sound horizon scale at the baryon drag epoch in a cosmology-independent way [13].

1.2. Shape or more lensing?

The curvature of the Universe could be considered an open issue, again. Lindley [18] explained that density of Universe is very close to the critical density, so it could be marginally open or closed. The Wilkinson Microwave Anisotropy Probe and Plank missions improved the analysis of CMB power spectra and found the results to be compatible with a flat Universe [19]. However, the last PL18 analysis led to an enhanced lensing amplitude in CMB power spectra that could be solved with a positive curvature at more than the 99% confidence [4, 20, 21].

A possible solution is found by connecting intrinsic and extrinsic global curvatures, since non-flat embedded manifolds can locally exhibit behaviours analogous to those of an intrinsically flat metric [6]. Positive curvatures of a linearly expanding Universe can be transformed to a radial inhomogeneity in space. This can then be projected as an acceleration of a homogeneous-flat hyperconical Universe by using some stereographic projection [22, 23]. This solution is not unique, but it is possible to define families of stereographic projections, applied to the hyperconical Universe. Under the intrinsic viewpoint of the resulting metric, this model can reproduce an apparent dark energy of $\Omega_\Lambda \approx 0.6937$, which is statistically compatible (0.9σ) with the PL18 results ($\Omega_\Lambda = 0.6889 \pm 0.0056$) [22].

1.3. Dark quantities or over-fitting parameters?

The well-known equivalence between acceleration and curvature was firstly used in General Relativity to solve classical physics in a geometrical way. Could the same idea solve cosmological tensions? The basic hypothesis is that accelerated expansion is a manifestation of the curvature of the Universe, by changing from extrinsic to intrinsic reference frames, or from other modified gravity metrics. That is, the apparent dark energy could be a purely geometrical effect caused by projecting embedded (inhomogeneous) hypersurfaces to maps of a (homogeneous) flat manifold. This idea leads to a modified gravity that is (at least locally) compatible with the standard model, as shown in [22, 23].

Similarly, at least part of the dark matter could actually be considered another geometrical effect of modified gravities, as is the case of modelling disc-galaxy rotation curves with MOND-TeVes theories [24, 25]. Furthermore, inconsistencies have been identified in different candidates of 'dark energy'. For instance, the Kilo-Degree Survey (KiDS-1000) showed differences with a 3σ tension with respect to the prediction of the CMB Planck Legacy analysis [26]. On the other hand, the observed cluster substructures are more efficient lenses than predicted by 'cold dark matter' (CDM) simulations, by more than an order of magnitude [27]. Moreover, the 'early dark energy' is a another key parameter proposed to solve the Hubble tension [8–10]. However, the large number of cosmological parameters are insufficient for

guaranteeing statistical robustness [28]. It might be possible that cosmology is undergoing the classical problem of epicycles.

1.4. Framework and structure of the study

This study is an extension of recent works developed in [6, 22, 23]. The first paper derived the extrinsic viewpoint and several intrinsic projections of a hyperconical manifold interpreted as a linearly expanding hypersphere embedded in four spatial dimensions and one time dimension. Observational compatibility was probed with 580 SNe Ia data collected from the Supernova Cosmology Project. This paper also showed that a purely positive curvature of the model ($k = 1$) is locally indistinguishable from that of a flat ΛCDM model ($\Omega_K = 0$). The second paper showed that dark energy can be interpreted geometrically as an apparent acceleration arising from by projecting the radial inhomogeneity of hyperconical universes. The paper determined the existence of a particular projection that makes the intrinsic hyperconical model to be regionally (2nd order) equal to the standard model, predicting $\Omega_\Lambda \approx 0.69$. Finally, the third paper explored the compatibility in local dynamics according to Lagrangian formalism and the Arnowitt–Deser–Misner (ADM) equations. This paper shows that a modified gravity Lagrangian density is required to ensure that the evolution of the metric is consistent at a local scale, identifying the only possibility of positive (extrinsic) curvature of $(k = 1)$, which is equivalent to the locally flat ΛCDM model. Here, we present an extension of the work through a derivation of two projection families to measure the boundaries of possible systematic errors of the model (beyond the initial prediction of $\Omega_\Lambda \approx 0.69$) and its application to explain some of the open issues of modern cosmology.

The present paper is structured into five parts: After this Introduction, the first technical section (2) describes the hyperconical model, its extrinsic definition and its projection or 'flattening' to obtain the intrinsic viewpoint like the standard model. Section 3 presents particular (explicit and numerical) solutions for equalising the projected hyperconical model and the standard model. Then, section 4 analyses the observational constraints of the model according to Pantheon Supernovae Type Ia sample as well as CCs and data based on radial BAO length methods in galaxy distribution. Finally, before concluding, section 5 discusses the unsolved aspects of the theory, such as the photon and baryon contents.

2. The hyperconical universe and its flattening

2.1. The model

We use the hyperconical model to explore possible solutions to the cosmological tensions. The key idea is based on the possibility of analysing our four-dimensional Universe from an **extrinsic viewpoint** (i.e. from the perspective of embedding in an ambient space with at least five dimensions) or from an **intrinsic viewpoint** (i.e. from the manifold metric, that represents the four-dimensional Universe). The first attempt is to consider the easier case of an homogeneous Universe (for instance, an hypersphere) expanding linearly. Then, the observer can find the adequate maps to translate the extrinsic to the intrinsic viewpoint of the metric.

To solve this, the derivation of the Friedmann–Lemaître–Robertson–Walker (FLRW) metric follows a separate process in terms of space and time. That is, it is firstly set the application from an open neighbourhood of the embedded object (in our case a hypersphere) and the reference system of the observer then, a scale factor (that depends on time) is applied. Contrarily to

the FLRW procedure, we consider that it would not be adequate to find spacetime-related maps in a separate way, as the expansion of the Universe (and of the observer) distorts the measures (see appendix A). In fact, our model showed that a simple linearly expanding hypersphere (i.e. the hyperconical Universe) becomes a radially-inhomogeneous curved Universe that can be easily projected to a flat accelerated Universe like the ΛCDM model [22].

2.2. Metric tensor

Let (t,ϕ,θ,γ) be four parameters with $t\subset\mathbb{R}_+:=(0,\infty)$, $\phi\subset[0,2\pi)$ and $\theta,\gamma\subset[0,\pi]$, used to define ordinary three-dimensional directions $\vec{e}_r:=(\sin\theta\cos\phi,\sin\theta\sin\phi,\cos\theta)\subset\mathbb{R}^3$ plus two-dimensional directions $(r,u):=(t\sin\gamma,t\cos\gamma)\subset\mathbb{R}^2$ or similarly $(r',u'):=(t_0/t)(r,u)$ for some set time $t_0\in\mathbb{R}_+$, therefore completing an ambient space $\mathbb{R}^3\times\mathbb{R}^2=\mathbb{R}^5$. Then, let $X:(t,\vec{e}_r,\gamma)\in U\subset\mathbb{R}^5\mapsto X_\gamma=(t,\vec{e}_r t\sin\gamma,t\cos\gamma)=:(t,\vec{r},u)\subset\mathcal{H}^4\subset\mathbb{R}^5$ be a path field over the hyperconical Universe $\mathcal{H}^4:=S^3_{\mathbb{R}_+}$, separated by an arc length γt with respect to an observer located at $\widehat{O}=(t_0,\vec{0},t)\in\mathcal{H}^4$. The differential path element $\mathrm{d}X$ is easily obtained taking into account that $\mathrm{d}\vec{r}'$ is decomposable in spherical coordinates as $\mathrm{d}\vec{r}'=\mathrm{d}r'\vec{e}_r+r'\mathrm{d}\Sigma'\vec{e}_\Sigma$, where $\mathrm{d}\Sigma'\vec{e}_\Sigma:=\mathrm{d}\theta'\vec{e}_\theta+\sin\theta'\mathrm{d}\phi\vec{e}_\phi$ is orthogonal to the radial direction $\vec{e}_r=\vec{r}/r$. The non-zero unshifted metric components $g_{\alpha\beta}$, for the observer $\widehat{O}$, are:

$$g_{t't'}=1 \tag{1}$$

$$g_{t'r'}=-a(t',r')^2\frac{1-(b-1)^2}{b^2\,(2(b-1)+1)}=-a(t',r')^2\frac{2-b}{2b^2-b} \tag{2}$$

$$g_{\theta\theta}=-a^2r'^2 \tag{3}$$

$$g_{\phi\phi}=-a^2r'^2\sin^2\theta \tag{4}$$

where $t':=t\sqrt{2b-1}$, $b:=\cos\gamma=\sqrt{1-r'^2/t_0^2}$, while $a(t',r')=t'/(t_0\sqrt{2b-1})$ is the scale factor. (see [6] for additional details).

2.3. Distorted reference frames

2.3.1. Comoving path. Let $Q_\gamma:(0,t_0]\subset\mathbb{R}\to\mathbb{R}^4$ be a comoving path located at the angle γ, and let $Q_\gamma(t)=Q(t):=(t,\vec{r}',u)\in\mathbb{R}^4$ be the position of any object with $\vec{r}=r\vec{e}_r$, $r^2:=\vec{r}\cdot\vec{r}$ and $\vec{e}_r:=\vec{r}/r$. Moreover, let $(\vec{r}',u'):=(t_0/t)(\vec{r},u)$ be the comoving spatial coordinates. Therefore, the position of any object can be expressed in spherical coordinates as follows:

$$Q(t)=\begin{pmatrix}t\\ \vec{r}\\ u\end{pmatrix}_{\hat{O}}=\frac{t}{t_0}\begin{pmatrix}t_0\\ \vec{r}'\\ u'\end{pmatrix}_{\hat{O}}=\frac{t}{t_0}\begin{pmatrix}t_0\\ t_0\sin\gamma\,\vec{e}_r\\ t_0\cos\gamma\end{pmatrix}=:Q_\gamma(t). \tag{5}$$

Then, each point $Q_\gamma(t)$ is projected to $Q_\gamma(t_0)$ by a line that passes through the point $\hat{O}(t_0):=(0,\vec{0},0)_{\hat{O}}$.

2.3.2. Distorted stereographic projection. Let $\alpha\in(0,1]$ be a free 'distortion parameter' and $\lambda\subset\mathbb{R}$ be a 'scale factor' that transforms time $t\mapsto\hat{t}:=t\lambda$ and distorts the comoving length $\hat{r}'$ as $r'\mapsto\hat{r}':=r'\lambda^\alpha$ for some set value of α. Moreover, let $F_Q:\mathbb{R}\to\mathbb{R}^5$ be a pencil with $F_Q(\lambda)\in\mathbb{R}^5$ parametrized such as $F_Q(1)=Q(t)=(t,\vec{r},u)$ and $F_Q(0)=\hat{Q}(0):=(0,\vec{0},u_0)$

with $u_0 := -t_0$. A transformation, given by $\vec{r}' = r'\vec{e}_r = t_0 \sin\gamma\, \vec{e}_r \mapsto \hat{r}'\vec{e}_r := t_0 \sin\hat{\gamma}\, \vec{e}_r$, is performed for the angles $\gamma \mapsto \hat{\gamma}$, preserving the direction $\vec{e}_r$. Therefore, following pencils are equivalent:

$$F_q^{(a)} \begin{cases} \hat{t} = t\lambda \\ \hat{r}' = r'\lambda^\alpha \\ \hat{u} = u_0 + (u-u_0)\lambda \end{cases} \quad \rightleftarrows \quad F_q^{(b)} \begin{cases} \hat{t} = t\lambda^{1/\alpha} \\ \hat{r}' = r'\lambda \\ \hat{u} = u_0 + (u-u_0)\lambda^{1/\alpha}. \end{cases}$$

When the points are projected on the hyperplane $\hat{u} = t_0$, a solution for the distorted stereographic projection is given by some $\lambda = \lambda_s(t,\gamma)$,

$$t_0 = -t_0 + (t\cos\gamma + t_0)\,\lambda_s \;\Rightarrow\; \lambda_s(t,\gamma) = \frac{2}{(1+\frac{t}{t_0}\cos\gamma)}. \tag{6}$$

Therefore, transformation $r' \mapsto \hat{r}' := r'\lambda^\alpha$ is reduced to find the value of α and the geometrical relation between time t and the comoving coordinate r' or γ. The value of α can be locally set by a dynamical constraint:

- Let $\{(q,p) \in \mathcal{C}^1(\mathbb{R}_{>0},\mathbb{R}^3) \times \mathcal{C}^1(\mathbb{R}_{>0},\mathbb{R}^3) \mid \gamma \in [0,\pi)\}$ be a dynamical system represented by symplectic coordinates (q,p), where $q := \vec{r}' = r'\vec{e}_r$ represents the position and $p := c_0\,\mathrm{d}\vec{r}'/\mathrm{d}t = c_0\,(\vec{e}_r \mathrm{d}r'/\mathrm{d}t + r'\mathrm{d}\vec{e}_r/\mathrm{d}t)$ is the conjugate momentum with some constant $c_0 \in \mathbb{R}_{>0}$. Assuming $\lambda \in \mathbb{R}$ as an independent parameter, spacetime transformation is locally $(\mathrm{d}t, \mathrm{d}r') \mapsto (\mathrm{d}\hat{t}, \mathrm{d}\hat{r}') = (\mathrm{d}t\,\lambda, \mathrm{d}r'\lambda^\alpha)$, so symplectic coordinates locally change as $(q,p) \mapsto (\hat{q},\hat{p}) = (q\lambda^\alpha, p\lambda^{\alpha-1})$, and the symplectic form

  $$\omega = \mathrm{d}q \wedge \mathrm{d}p = \mathrm{d}\hat{q} \wedge \mathrm{d}\hat{p} = \mathrm{d}q \wedge \mathrm{d}p\,\lambda^{2\alpha-1} \tag{7}$$

  should be locally conserved. For the simple comoving case ($p = 0$), it is found that $\omega = 0$ for every $\alpha \in \mathbb{R}$. Otherwise, it is necessary to set $\alpha = \alpha_s \equiv 0.5$ for dynamical systems with $p \neq 0$ and $\lambda \neq 1$.

2.3.3. Local time relationship. Each hypersphere of radius t is locally projected (expanded) to the hyperesphere of radius $t_0 > t$ by distorting the spatial coordinates $\vec{r}'$. Extra-dimension u' should disappear taking some adequate reference chart (e.g. by using polar coordinates or using a flattening projection).

Taking into account the inhomogeneous scale factor related to redshift z (see [6]),

$$\frac{t}{t_0} = \frac{1}{1+z} \approx \sum_{n=0}^{\infty} b_n \left(\frac{r'}{t_0}\right)^n = 1 - b_1\frac{r'}{t_0} + O\left(\frac{r'^2}{t_0^2}\right) \;\text{ with }\; b_1 = 1 \tag{8}$$

with $b_1 = 1$ at a local neighbourhood, the projection parameter is found:

$$t_0 = -t_0 + (t\cos\gamma + t_0)\,\lambda_s \;\Rightarrow\; \lambda_s(t(\gamma),\gamma) \approx \frac{2}{(1+\left(1-\sin\gamma + b_\ell \sin^2\gamma\right)\cos\gamma)} \tag{9}$$

where b_ℓ is a fitting parameter that depends of the spatial scale considered. For very local scales ($\gamma << 1$), it is useful to approximate equation (9) as

$$\lambda_s(t(\gamma),\gamma) \approx \frac{1}{1-\frac{\gamma}{2}}. \tag{10}$$

2.3.4. Global time relationship. Applying $\gamma = 0$ to the $t(\gamma)$ relationship before the projection, the extra-dimension u logically satisfies the condition of that $(t_0/t)u = \lambda_s u = \hat{u}$ because

$t(0)=t_0$. However, in general $\lambda_s \neq t_0/t$, and non-zero differences $D:=((t_0/t)u-\hat{u})/\hat{t}\neq 0$ are found for $\gamma>0$. A global approach for the $t(\gamma)$ relationship can be derived by assuming that there exists an apparent maximum angle $\gamma_0\in\mathbb{R}_+$ such as $D=1$. Linearly with γ, the $t(\gamma)$ relationship can be estimated as follows:'

$$(t_0\lambda^{-1}-t)\cos\gamma \approx t_0\gamma/\gamma_0. \tag{11}$$

With this, equation (6) is:

$$t_0 \approx -t_0+\left(t_0\left(\frac{1}{\lambda}-\frac{\gamma}{\gamma_0\cos\gamma}\right)\cos\gamma+t_0\right)\lambda_u \quad\Rightarrow\quad \lambda_u\approx\frac{2-\cos\gamma}{1-\frac{\gamma}{\gamma_0}}\sim\frac{1}{1-\frac{\gamma}{\gamma_0}}. \tag{12}$$

On the other hand, the relative difference $(t_0\lambda_s^{-1}-t)/t_0\in(0,1)$ should be at the maximum when the domain limit $\gamma\to\pi/3$ is reached (see, for instance, [22]); herefore $\gamma_0=(\pi/3)/\cos(\pi/3)=2\pi/3\approx 2.09$. In contrast, by equaling the hyperconical-based Hubble parameter to the ΛCDM-dependent one [22], it is analytically found that

$$\alpha=\frac{5}{18}\gamma_0(1+\epsilon) \;\rightarrow\; \gamma_0=\frac{18}{5(1+\epsilon)}\alpha \tag{13}$$

for some $|\epsilon|<1/2$. For example, one finds $\epsilon=0$ when the hyperconical-based Hubble parameter is compared to the ΛCDM-dependent Hubble parameter up to third order [22], and $\epsilon=-\frac{1}{10}$ for the local approach ($\gamma_0=2$ from equation (10) and therefore $\gamma_0=4\alpha$, with $\alpha=0.5$).

3. Particular theoretical solutions

By applying the Taylor–Maclaurin expansion to both ΛCDM and hyperconical Hubble parameters (around the point at $\gamma=0$), system of equations are obtained up to the second order depending on the (global or local) approach considered. Applying equation (10) to the ($\alpha=0.5$)-distorted projection and comparing to a simple ΛCDM model with $\Omega_r=0=\Omega_K$, it is locally found

$$\Omega_\lambda=\frac{2}{3},\;\; \Omega_m=\frac{1}{3},\;\; b_\ell=-\frac{5}{8}. \tag{14}$$

A third-order global approach can be applied for $\Omega_K\neq 0$. Under this approach, $\lambda=\lambda_u$ (equation (12)) and the angle $\gamma_0=2(1+\delta)$ is rewritten for some $|\delta|<0.05$ to allow γ_0 ranging close to 2 and 2.09 (e.g. from local to global approaches), while the distortion parameter α is expressed as $\alpha=\frac{5}{18}\gamma_0(1+\epsilon)$. If $\epsilon=0$ is considered (appendix B.5.3),

$$\begin{aligned}
\Omega_\Lambda &= \frac{1}{1+\delta}\left(\frac{13}{18}+\frac{11}{36}\delta-\frac{5}{9}\delta^2\right)-\frac{1}{3}\Omega_r\\
\Omega_m &= \frac{1}{1+\delta}\left(\frac{1}{3}-\frac{1}{2}\delta-\frac{10}{9}\delta^2\right)-\frac{8}{3}\Omega_r\\
\Omega_K &= \frac{1}{1+\delta}\left(-\frac{1}{18}+\frac{43}{36}\delta+\frac{5}{3}\delta^2\right)+2\Omega_r,
\end{aligned} \tag{15}$$

where $\delta=\pi/3-1$ can be taken if $\gamma_0=2\pi/3$. In particular, for $\Omega_r=0=\Omega_k$, two solutions of δ are found ($\delta\approx-0.76$ and $\delta\approx 0.044$ corresponding to $\gamma_0\approx 0.49$ and $\gamma_0\approx 2.09\approx\frac{2}{3}\pi$) with both displaying the same matter $\Omega_m\approx 0.30$ and dark energy $\Omega_\Lambda\approx 0.70$. However, $|\delta|<0.05$

is rejected by hypothesis. Similar results regarding dark energy/matter are found if $0 < \epsilon \leqslant \delta$ is restricted with a unique solution. For instance, with $\epsilon = \delta$ and $\Omega_r = 0$,

$$\begin{aligned}\Omega_\Lambda &= \frac{13}{18} - \frac{25}{54}\delta + O(\delta^2)\\ \Omega_m &= \frac{1}{3} - \frac{55}{27}\delta + O(\delta^2)\\ \Omega_K &= -\frac{1}{18} + \frac{5}{2}\delta + O(\delta^2).\end{aligned} \tag{16}$$

The third-order contact point with $\Omega_r = 9.0(5) \times 10^{-5}$ and free Ω_K leads to similar dark energy values ($\Omega_\Lambda = 0.7032\ 646(20)$), but a ΛCDM-closed Universe ($\Omega_K = -0.015\ 07(1)$) with more apparent dark matter ($\Omega_m = 0.311\ 715(20)$). The emerging curvature coincides with the low distorting factor $\alpha = 0.573$ compared to $\alpha \approx 0.5765(1)$ obtained for an almost flat Universe ($\Omega_K = -0.008\ 240(16)$). Similar results are found for the second-order global approach: the minimum distorting factor $\alpha = 5/9$ leads to a higher positive curvature ($\Omega_k = -1/18$) compared to $\alpha = 0.579\ 857\ 642(1)$, which is obtained by setting $\Omega_k = 0$ (see appendix B). These findings are in concordance with the observation that a closed Universe can provide a physical explanation for avoiding the so enhanced lensing factor [21].

The curvature value is separated with respect to the best fit of PL18 temperature power spectra ($\Omega_K = -0.045(15)$), but is within the confidence level when lensing data are added ($\Omega_K = -0.012(6)$) and also within the limits from the combination of Planck CMB temperature, polarization, and lensing power spectra ($\Omega_K = -0.0096(61)$). If BAO data is considered, the curvature is closed to zero but statistically compatible with positive values ($\Omega_K = 0.0007 \pm 0.0019$). In sum, the constraints from the PL18 CMB spectra on curvature, parameterized through the energy density parameter lead to $0.007 > \Omega_K > -0.095$ at the 99%. The best PL18 fitting ($\Omega_K = -0.045(15)$) is only compatible with the modelled values under second-order contact point ($\Omega_K = -1/18 \approx -0.055$) (table 1). The predicted value of $\Omega_K = -1/18$ is also aligned to the estimations of $\Omega_K = -0.07^{+0.12}_{-0.15}$ and $\Omega_K = -0.076 \pm 0.012$ found by combining CCs and BAO data [29, 30].

4. Observational compatibility

4.1. Local-to-global tensions

The significant difference or not between local and global values of the expansion rate H_0 is a key feature that distinguishes between homogeneous and inhomogeneous spaces. Specifically, our model suggests that apparent acceleration emerges when a radially inhomogeneity is projected in a homogeneous chart (as found in [22]). This phenomenon is similar to that one showed by Kovács *et al* [35]: by using the inhomogeneous Average Expansion Rate Approximation (avERA) model, Hubble tension can be explained without dark energy.

In fact, the local-to-global ratio $H_0(L)/H_0(G) = 1$ is the well-known $\Omega_\Lambda = 0.72(1)$ solution found by [36], which is very close to our theoretical value of $\Omega_\Lambda = 0.7375(4)$, produced by the equality $F_t := t_0 H_0 \equiv 1$ between the age of Universe age (t_0) and the Hubble time ($1/H_0$), globally and without any projection [6].

The hyperconical model assumes a factor $F_t \equiv 1$ (that is $H_0 \equiv 1/t_0 \approx 71.0\,\mathrm{km\,s^{-1}\,Mpc^{-1}}$ assuming PL2018+BAO $t_0 \approx 13.810^9$ years), as a Universe expansion driven by the course of time. This natural expansion leads to a distant/local ratio values of Hubble parameter as $\rho_z := H(z)/H_0 = 1 + z$, which is compatible with the observations of Riess *et al* [37]. For

Table 1. Intrinsic-viewpoint prediction: apparent cosmological parameters by equivalence between ΛCDM and (projected) hyperconical models for second- and third-order contact point, and considering local (L) and global (G) approaches. The last significant figure error is shown in parentheses and bold indicates that the parameter is set, not adjusted. The Hubble parameter ($H_0\,\mathrm{km^{-1}\,s^{-1}Mpc^{-1}}$) is directly obtained from the *time factor* (F_t) assuming an age of $13.80(3)\cdot 10^9$ years.

Parameter	2nd order(L), $\Omega_K=0$	2nd order(G), $\Omega_K\neq 0$	2nd order(G), $\Omega_K=0$	3rd order(G), $\lvert\epsilon\rvert<\lvert\delta\rvert$	3rd order(G), $\lvert\epsilon\rvert>\lvert\delta\rvert$	3rd order(G), $\epsilon=\delta$
ϵ	0.081 776(1)	**0** (set)	−0.003 44(1)	−0.014 82(1)	0.034 462(4)	0.018 718(2)
δ	—	**0** (set)	$\frac{\pi}{3}-\mathbf{1}$ (set)	$\frac{\pi}{3}-\mathbf{1}$ (set)	**0** (set)	0.018 718(2)
α	**0.5** (set)	$\frac{5}{9}\approx 0.555$	0.579 857 642(1)	0.5731(1)	0.574 66(4)	0.5765(1)
Ω_K	**0** (set)	$\frac{-1}{18}\approx -0.055$	**0** (set)	−0.015 070(17)	−0.011 819(15)	−0.008 240(16)
Ω_r	**0**(*set*)	**0**(*set*)	$\mathbf{9.0}(5)\cdot 10^{-5}_{(set)}$	$\mathbf{9.0}(5)\cdot 10^{-5}_{(set)}$	$\mathbf{9.0}(5)\cdot 10^{-5}_{(set)}$	$\mathbf{9.0}(5)\cdot 10^{-5}_{(set)}$
Ω_m	$\frac{1}{3}\approx 0.333$	$\frac{1}{3}\approx 0.333$	0.297 517 827(1)	0.311 715(20)	0.304 056(17)	0.294 737(18)
Ω_Λ	$\frac{2}{3}\approx 0.667$	$\frac{13}{18}\approx 0.722$	0.702 482 173(1)	0.7032 646(20)	0.707 674(4)	0.713 413(3)
F_t	0.935 881(1)	0.951 745(1)	0.9663 756(1)	0.9579 073(17)	0.963 691(4)	0.971 050(3)
H_0	66.38(10)	67.50(10)	68.54(11)	67.94(11)	68.35(12)	68.87(13)

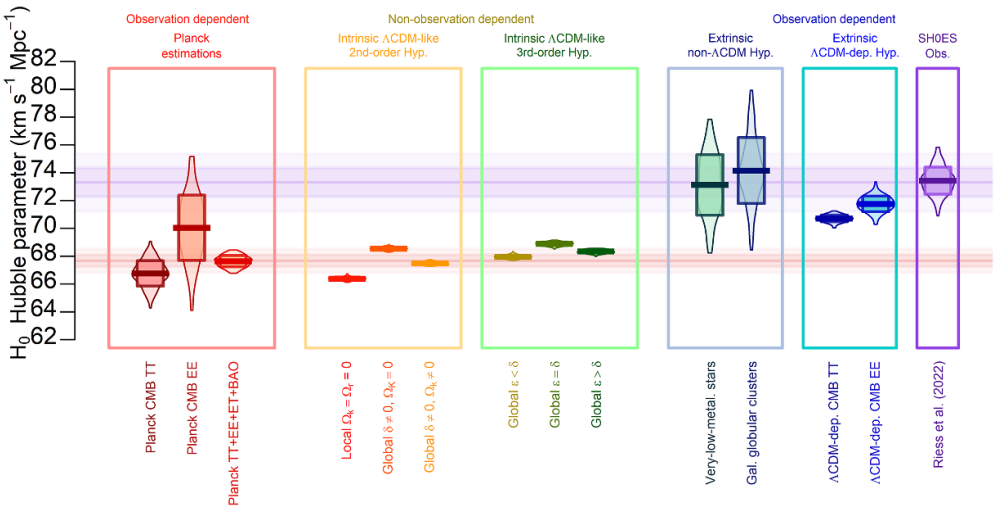

Figure 1. Hubble parameter estimated under intrinsic viewpoint, with local (orange box) or global (green box) approaches, and under extrinsic viewpoint (blue boxes) of the Hyperconical model, compared to ΛCDM-dependent Planck legacy (left red box) and SH0ES observations (right purple box), which is obtained by 'cosmic distance ladder' (a chain of direct methods).

instance, the estimated value of $\rho_{1.5} = H(z = 1.5)/H_0 = 2.69^{+0.86}_{-0.52}$ is in agreement with our predicted value of $\rho_{1.5} \equiv 2.5$.

When the hyperconical Universe is forced by flattening to reproduce the ΛCDM model, the estimation of time factor is reduced ($F_t < 1$) due to an apparent (emerging) acceleration, which reproduces a minimum value of H_0 at a local scale (second-order contact point) with values very close to the Planck observations.

The corresponding local observation in CMB is the Planck temperature (TT) power spectrum. The CMB TT results provided low values of dark energy density ($\Omega_\Lambda = 0.679(13)$) compatible with our local prediction of $\Omega_\Lambda \approx 0.667$ (table 1). Under the global approach with a three-order contact point, the increase of the distorting parameter ($\alpha > 0.5$) producing an increase of the dark energy $\Omega_\Lambda > 0.7$ and a curvature reduction down to $|\Omega_K| < 0.02$.

These values are comparable with the CMB polarisation power spectrum (EE), because they are non-linear (non-Gaussian) and do not depend on the coordinates (global-like approach) (figure 1). Particularly, CMB EE power spectra showed higher values of dark energy $\Omega_\Lambda = 0.711(30)$ with Hubble parameter about $69.9 \pm 2.7\,\mathrm{km\,s^{-1}\,Mpc^{-1}}$ and the corresponding value from the linear hyperconical model ($H_0 = 1/t_0$) is $71.69 \pm 0.65\,\mathrm{km\,s^{-1}\,Mpc^{-1}}$ (table 2), which are compatible with the values estimated with Large Magellanic Cloud (LMC) Cepheid samples, of about $H_0 = 73 \pm 1\,\mathrm{km\,s^{-1}\,Mpc^{-1}}$ (SH0ES [2, 3, 38]). In fact, the SH0ES estimation leads to an independent-scale ratio of 1.037 ± 0.036 and a time factor of $F_t = 0.97 \pm 0.05$.

In summary, our interpretation of the Hubble tension is that cosmology-dependent measurements are strongly influenced by the intrinsic viewpoint of the models used. This is the case of the CMB EE/TT power spectra, most of BAO-based methods and the luminosity distance of SNe Ia among others. In other words, the constraints are applied to a FLRW metric inadequately derived for moving reference frames (see appendix A). In contrast,

Table 2. Extrinsic-viewpoint prediction. The values of the Hubble parameter (H_0 in $\mathrm{km\,s^{-1}\cdot Mpc^{-1}}$) according to the linear expansion (unprojected Hyperconical model [6]) by using several ages of the Universe ($t_{\hat{o}}$ in 10^9 years) and statistical tensions with respect to the most current local observations: $H_0 = 73.30 \pm 1.04\,\mathrm{km\,s^{-1}Mpc^{-1}}$ (SH0ES, LMC-CS) [3] and $69.8 \pm 1.7\,\mathrm{km\,s^{-1}Mpc^{-1}}$ (TRGB) [31] at 68% C.L.

Age estimation technique	$t_{\hat{o}}$	$H_0 = 1/t_{\hat{o}}$	σ/ [3]	σ/ [31]
Very-low-metallicity stars [32]	13.40(45)	73.0 (2.1)	0.1	1.5
Galactic globular clusters [33, 34]	13.2(4)	74.1 (2.4)	0.3	1.8
ΛCDM-dependent TT [20]	13.83(37)	70.71(26)	2.5	0.5
ΛCDM-dependent EE [20]	13.64(15)	71.69(65)	1.5	1.1
ΛCDM-dependent TT, TE, EE [20]	13.80(24)	70.86(40)	2.3	0.6

cosmology-independent observations such as the purely geometric approaches such as the SNe distance ladder would be more influenced by extrinsic geometry. Observe that the distance ladder method propagates the 'very local scale' to larger scales through a chain of correlated/overlapped methods, bridging the contrast produced by the distorted stereographic projection (intrinsic viewpoint) and therefore it leads to practically unprojected measurements.

4.2. Observational constraints of the projected model with SNe Ia

An estimation of ϵ and α was obtained according to 1048 Type Ia supernovae (SNe Ia) in the range of $0.0101 < z < 2.26$ and collected from the Pantheon sample [39, 40]. This dataset contains both the heliocentric redshift (z_{hel}, direcly observed redshift) and the CMB-frame redshift (z_{CMB}) obtained from standard procedures; that is, the CMB-frame redshift is the redshift after the correction of the Planck-observed CMB dipole caused by the particular velocity of our galaxy plus Solar System with respect to the CMB. Taking into account the fact that the standard luminosity distance $\mathrm{d_L}$ depends on the combination of both redshifts [40, 41], for the KΛCDM model, one can use

$$d_{\mathrm{L}} = (1+z_{\mathrm{hel}})\,r' = \mathrm{sin}_K \int_0^{z_{\mathrm{CMB}}} \frac{\mathrm{d}z}{H_0\sqrt{\Omega_m(1+z)^3+\Omega_K(1+z)^2+\Omega_\Lambda}} \tag{17}$$

where $\mathrm{sin}_K x := \lim_{\epsilon\to K} \frac{\sin(\sqrt{\epsilon}x)}{\sqrt{\epsilon}}$, $K = -\Omega_K H_0^2$; i.e. $\mathrm{sin}_0\, x = x$, $\mathrm{sin}_{+1}\, x = \sin x$, $\mathrm{sin}_{-1}\, x = \sinh x$.

The hyperconical model predicts a Pearson's chi-squared value of $\chi^2 = 1031.1$ with a cumulative probability of $p_\chi := p(\chi^2 \leqslant \chi_0^2) = 36.9\%$, which is practically equal to the KΛCDM model fit ($\chi^2 = 1031.7$, $p_\chi = 37.4\%$) and slightly lower than the ΛCDM standard model result ($\chi^2 = 1037.0$, $p_\chi = 42.0\%$). The best-fit parameters of the proposed model are $\alpha = 0.499(13)$ with a general fit of $\alpha > 0.1$ and $\epsilon = 0.1 \pm 0.2$ (σ levels), which corresponds to $\gamma_0 = 1.6^{+0.4}_{-0.2}$ (figure 2). The distortion exponent is consistent with the theoretical local-value of $\alpha = 0.5$, but the maximum angle is deviated with respect to the expected value of $\gamma_0 = \frac{18}{5}\alpha/(1+\epsilon) \approx \frac{2}{3}\pi$, although close to the local value of $\gamma_0 = 2$ (see equation (10)).

4.3. Observational constraints of the projected model with CC and BAO data

A sample of 34 CCs and 7 values from radial BAO size in galaxy distribution (BAO-Gal) was collected in table 3 to model the Hubble parameter (H) as a function of the redshift (z). Omitting the effects of radiation ($\Omega_r \approx 0$) and curvature ($\Omega_K \approx 0$) at $z \leqslant 1$, one-parameter models were

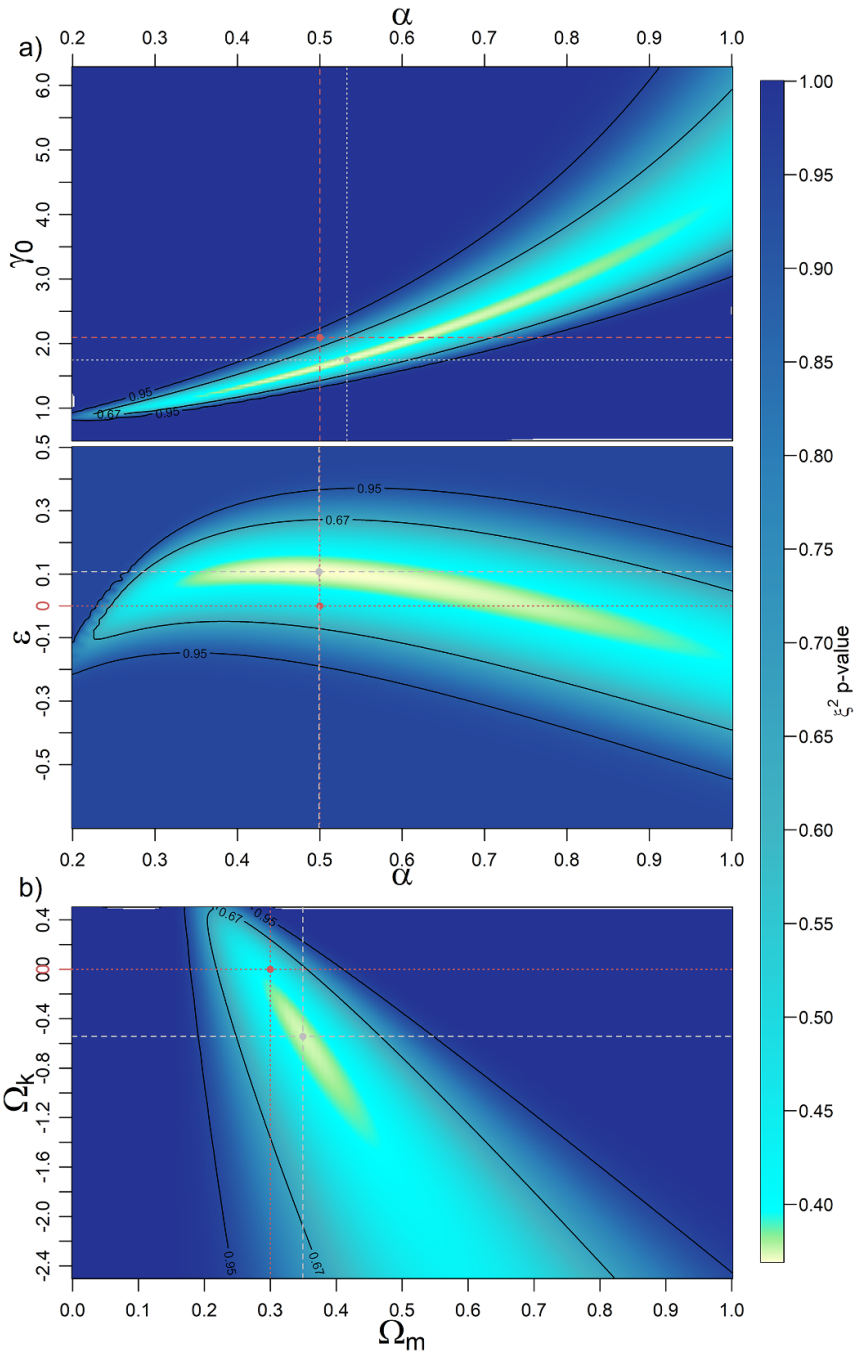

Figure 2. Observational constraints (chi-square p-value) for (a) the Hyperconical model with parameters (α, γ_0) or (α, ϵ), and (b) the KΛCDM model, according to the Pantheon sample [39, 40]. The red dots and dotted lines represent theoretical values, while the grey dots and dashed lines marks the best fit in any case. The 95% and 67% confidence levels are highlighted by black continuous contour lines.

Table 3. Hubble parameter (H) and statistical error (σ) estimated by using Cosmic Chronometers (CC) and radial BAO size from galaxy distribution (BAO-Gal).

z	$H(z)$ km^{-1}s^{-1} Mpc^{-1}	$\pm1\sigma(H(z))$	Method	Reference
0.0708	69.0	19.68	CC	Zhang *et al* (2014) [44]
0.09	69.0	12.0	CC	Jimenez *et al* (2003) [45]
0.12	68.6	26.2	CC	Zhang *et al* (2014) [44]
0.17	83.0	8.0	CC	Simon *et al* (2005) [46]
0.179	75.0	4.0	CC	Moresco *et al* (2012) [47]
0.199	75.0	5.0	CC	Moresco *et al* (2012) [47]
0.2	72.9	29.6	CC	Zhang *et al* (2014) [44]
0.240	79.69	2.65	BAO-Gal	Gaztan aga *et al* (2009) [48]
0.27	77.0	14.0	CC	Simon *et al* (2005) [46]
0.28	88.8	36.6	CC	Zhang *et al* (2014) [44]
0.35	84.4	7.0	BAO-Gal	Xu *et al* (2013) [49]
0.352	83.0	14.0	CC	Moresco *et al* (2012) [47]
0.3802	83.0	13.5	CC	Moresco *et al* (2016) [50]
0.4	95.0	17.0	CC	Simon *et al* (2005) [46]
0.4004	77.0	10.2	CC	Moresco *et al* (2016) [50]
0.4247	87.1	11.2	CC	Moresco *et al* (2016) [50]
0.43	86.45	3.68	BAO-Gal	Gaztan aga *et al* (2009) [48]
0.44	82.6	7.8	BAO-Gal	Blake *et al* (2012) [51]
0.4497	92.8	12.9	CC	Moresco *et al* (2016) [50]
0.47	89	50	CC	Ratsimbazafy *et al* (2017) [52]
0.4783	80.9	9.0	CC	Moresco *et al* (2016) [50]
0.48	97.0	62.0	CC	Stern *et al* (2010) [53]
0.57	92.4	4.5	BAO-Gal	Samushia *et al* (2013) [54]
0.593	104.0	13.0	CC	Moresco *et al* (2012) [47]
0.6	87.9	6.1	BAO-Gal	Blake *et al* (2012) [51]
0.68	92.0	8.0	CC	Moresco *et al* (2012) [47]
0.73	97.3	7.0	BAO-Gal	Blake *et al* (2012) [51]
0.75	98.8	33.6	CC	Borghi *et al* (2022) [15]
0.8	113.1	15.1	CC	Jiao *et al* (2023) [55]
0.781	105.0	12.0	CC	Moresco *et al* (2012) [47]
0.875	125.0	17.0	CC	Moresco *et al* (2012) [47]
0.88	90.0	40.0	CC	Stern *et al* (2010) [53]
0.9	117.0	23.0	CC	Simon *et al* (2005) [46]
1.037	154.0	20.0	CC	Moresco *et al* (2012) [47]
1.26	135	65	CC	Tomasetti *et al* (2023) [16]
1.3	168.0	17.0	CC	Simon *et al* (2005) [46]
1.363	160.0	33.6	CC	Moresco (2015) [56]
1.43	177.0	18.0	CC	Simon *et al* (2005) [46]
1.53	140.0	14.0	CC	Simon *et al* (2005) [46]
1.75	202.0	40.0	CC	Simon *et al* (2005) [46]
1.965	186.5	50.4	CC	Moresco (2015) [56]

considered in this paper to be adjusted to the measurements. For instance, the Hubble parameter of the standard model (e.g. $\Omega_\Lambda \approx 0.70$, $\Omega_m \approx 0.30$) and the equivalent projection of the hyperconical model (e.g. 3rd-order approach) can be simply represented by

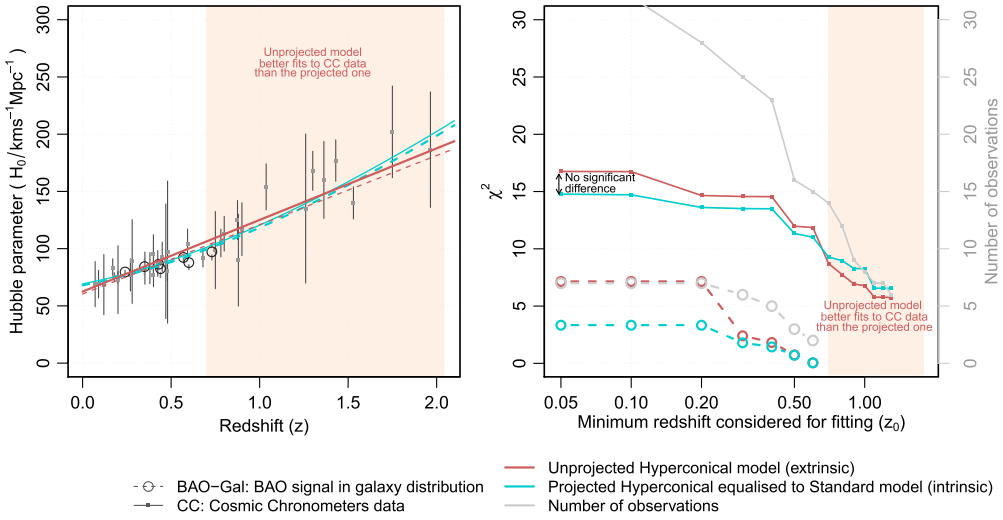

Figure 3. (Left): Fits of the unprojected and projected hyperconical models to the observations the Hubble parameter estimated from cosmic chronometers and radial BAO size methods, respectively. (Right): Interpretation of Pearson chi-squared statistics (χ^2) obtained for the fits restricted by $z > z_0$ with respect to a particular threshold z_0.

$$H_{\rm proj}(z) \approx H_{\rm stan}(z) :\approx H_{0,\rm stan}\sqrt{\Omega_m(1+z)^3+\Omega_\Lambda}\ . \tag{18}$$

Although redshift is assumed to be affected by the intrinsic geometry, we also employ the unprojected hypercone to compare. Since it expands linearly, its Hubble parameter is exactly

$$H_{\rm unpr}(z) := H_{0,\rm unpr}(1+z)\ . \tag{19}$$

Taking the sample of 7 values from the BAO signal in galaxy distribution, the performance of the standard model (and the equivalent projection of the hyperconical model) is clearly better than the unprojected model. Specifically, the standard cosmology obtains $\chi^2 = 3.3$ and $p_\chi = 23\%$ while the unprojected model provides $\chi^2 = 7.2$ and $p_\chi = 69\%$ (figure 3). However, if other methods are considered to constraint the BAO sound horizon scale (e.g. Lyα forest spectra), the new values of H_0 are incompatible with the unprojected model. Specifically, Font-Ribera *et al* [42] estimated $H_0 = 226\ \pm\ 8$ at $z = 2.36$ and Delubac *et al* [43] found $H_0 = 222\ \pm\ 7$ at $z = 2.36$ under the BAO-Lyα approach. Considering BAO-Gal+BAO-Lyα (9 values), the standard model obtains $\chi^2 = 6.5$ and $p_\chi = 41\%$ while the unprojected model provides $\chi^2 = 17.7$ and $p_\chi = 98\%$, which is rejected at a 0.05 level of significance.

Considering the sample of 34 purely cosmology-independent CC values, projected and unprojected models show closer Pearson Chi-squared statistics, $\chi^2 = 14.8$ and $\chi^2 = 16.8$ respectively, that correspond to $p_\chi = 0.3\%$ and $p_\chi = 0.8\%$. For the sub-sample of 8 CC points restricted at $z > 1$, it was obtained $\chi^2 = 6.8$ with $p_\chi = 55\%$ for the unprojected model, and $\chi^2 = 8.3$ with $p = 69\%$ for the standard model. In short, the unprojected and projected approaches are statistically indistinguishable for CC data but not for the BAO signal.

Concerning the Hubble parameter constraint, $H_0 = h_0\,\mathrm{km\,s^{-1}Mpc^{-1}}$, the standard model leads to $h_0 = 66.72\ \pm\ 0.65$ for BAO-Gal+BAO-Lyα data (9 points), $h_0 = 68.0\ \pm\ 1.1$ for only BAO-Gal (7 points) and $h_0 = 69.3\ \pm\ 1.3$ for the CC sample (34 points). That is a 2σ-higher expansion rate measured in CC than in BAO-Gal+BAO-Lyα. This tension disappears

when Lyα data is dropped. If the CC sample is restricted at $z > 1$, the best fit of the standard model increases the Hubble parameter to $h_0 = 71.3 \pm 3.1$ versus $h_0 = 68.6 \pm 1.1$ for $z < 0.5$. All these small tensions between the local ($z < 0.5$) and larger ($z > 1$) scales are aligned to the results showed in table 3.

5. Weak points to be further analysed

As weaknesses of the theory, the hyperconical model cannot predict the visible matter content or the photon density. In fact, to analyse the first acoustic peak (from the photon-baryon decoupling), it is necessary to introduce photons into the model. Moreover, the selection of the projection family is not unique but several possible solutions that are compatible with Supernovae Type-Ia observations and ΛCDM fitting. Nevertheless, the proposed model needs to be validated with more sets of observational data.

The possible impacts of our theory on local gravity (e.g. galaxy rotation curves) are still unexplored. The problem of embeddings construction for gravity metrics has been analysed in many studies [57, 58]. According to the Kasner's theorem, any vacuum solution of the Einstein equations needs to be embedded into at least a six-dimensional ambient space [58]. However, we only used five dimensions to model the Universe large-scale features, without matter contents. Further works should integrate transition way between five-dimensional large-scale effects and six-dimensional local perturbation metrics or, at least, a procedure to reproduce these effects as a limit case of a more general theory. For instance, the ADM decomposition allows to compare Kerr-Child metrics to embed time-constant hypersurfaces, which are spacelike or Cauchy hypersurfaces, into a flat four-dimensional space (plus the temporal dimension) [59]. Therefore, Einstein field equations (and their solutions) would actually be an approach that has the same limit case as the linear perturbation of the background metric.

Finally, the model is in its early stage of development, with simple assumptions of distorted stereographic projections and local-to-global approaches for the time dependence. The search for the of values for its parameters should be contrasted with more observational sets, and the analysis should be expanded to better understand the differences found when BAO-Gal or CC samples (cosmology-independent data) are used.

6. Conclusions

Currently, standard cosmology presents a list of problems that are difficult to solve without the addition of new parameters that could lead to overfitting effects. Among others, the list includes incompatible estimations of the Hubble parameter ('Hubble tension'), a Universe density that is practically equal to the critical density ('flatness problem') and a dark matter estimated in CMB Planck mission that is excessive and/or inconsistent with estimations from galaxies. This paper shows that most of the issues raised can be solved by modifying the initial hypothesis to derive the Universe (FLRW) metric.

Particularly, we applied a mathematical prescription to derive the Universe manifold $(\mathbb{R}^4, g)$ by embedding it into a higher-dimensional space $(\mathbb{R}^5, \eta)$ with the Minkowskian metric η. To determine possible solutions at an early stage, we first suppose the most simple case, a **homogeneous finite object with linear expansion**. For instance, we consider a hypersphere S^3_t with radius equal to the age $t \in \mathbb{R}_{\geqslant 0}$ of the Universe, embedded into the Cartesian product of its time ($\mathbb{R}_{\geqslant 0}$) and its purely four-dimensional space $\mathbb{R}^4$, that is a hyperconical object $\mathcal{H}^4 := S^3_{\mathbb{R}_{\geqslant 0}} \subset \mathbb{R}_{\geqslant 0} \times \mathbb{R}^5$. By applying a time transformation of the reference frames,

a radially inhomogeneous and closed Universe ($\mathcal{H}^4$) is obtained for a given observer, it is possible to model the above-mentioned cosmological problems.

To attain our goal, two additional hypotheses were considered: (a) the Universe shape does not depend on matter content, (b) there exists a locally conformal projection that absorbs the curvature as an acceleration. That is, dark energy could be purely interpreted as a geometric manifestation of the intrinsic curvature of the Universe.

This equivalence was tested by two parametric families of stereographic projections according to local and global approaches. The result is a Hubble expansion law compatible with the SH0ES estimations, under the extrinsic viewpoint; and another Hubble parameter compatible with the ΛCDM model up to third order of series expansion, under an intrinsic viewpoint. Therefore, it is proposed that Hubble tension can be explained as an effect of both geometrical perspectives: On the one hand, compared to the Plank Legacy estimation of $h_0 = 67.4 \pm 0.5$ [4], our intrinsic ΛCDM-based compatibility leads to a Hubble parameter between 66.38 and 68.87 by using the estimation of the age (13.80×10^9 years) as a necessary parameter. On the other hand, with ΛCDM-independent observations (e.g. very-low-metallicity stars and galactic globular clusters), the extrinsic viewpoint of our model predicts a Hubble parameter between 73 and 74, which is compatible with the value of $h_0 = 73.30 \pm 1.04$, estimated with the distance ladder method applied to the Cepheid-SNe sample [2, 3]. The explanation of why distance ladder is extrinsic is that technique propagates the 'local scale' to larger scales through a chain of correlated and overlapped methods, bridging the contrast produced by the distorted stereographic projection (intrinsic viewpoint) and therefore leading to practically unprojected measurements.

If galaxies are taken into account (e.g. CCs and radial BAO size methods), the extrinsic viewpoint underestimates the Hubble parameter at local scales ($h_0 < 65$ at $z < 0.5$) but it is compatible with the intrinsic modelling at larger scales ($h_0 \approx 70$ at $z > 1$).

Collaterally, the fitted values of cosmological parameters are interpreted as apparent density values, different to the real matter contents (baryonic and radiation). That is, apparent dark quantities (energy and matter) emerged from our model without considering any kind of matter content. Particularly, dark energy densities (Ω_Λ) between $\frac{2}{3} \approx 0.667$ and $\frac{13}{18} \approx 0.722$ emerge when curvature is set to zero ($\Omega_K = 0$) or is freely nonzero ($\Omega_K = -1/18 \approx -0.055$), while third-order model-compatibility leads to the following values: $\Omega_\Lambda = 0.708 \pm 0.005$ and $\Omega_K = -0.012 \pm 0.003$.

As a final remark, a question about possible alternative models is raised: following the simplest example of the homogeneous finite sphere embedded in a upper-dimensional flat manifold, is it possible to build an infinite flat Universe in a finite time? Dynamical embedding described in this paper allows a projection to simulate it from linear-expanding closed universes.

Data availability statement

No new data were created or analysed in this study.

Acknowledgment

During the preparation of this work, RCS was financially supported by the research project MTM2016-79422-P of the AEI/FEDER (EU). We are also grateful to two anonymous reviewers for helpful comments. The very-helpful comments and suggestions received from the anonymous reviewers are also gratefully acknowledged.

Appendix A. Theoretical derivation of the hyperconical metric

This annex aims to show two fundamental linked points of the present work: (a) the FLRW metric is derived combining an static manifold and a time dimension, which is not adequate since it omits the effects of an observer that lives in a moving reference frame. (b) The derivation of the hyperconical model in a similar way to the FLRW metric but without setting a static reference frame, chosen as a more suitable alternative to solve some open issues in cosmology.

To facilitate the reading, a three-dimensional case is considered first. Let φ be a map from spherical coordinates $p=(\gamma,\phi,\theta)\in\mathbb{R}^3$ to a hypersphere $S^3_{t_0}\subset\mathbb{R}^4$ of radius t_0 given by

$$\begin{aligned}\varphi:\mathbb{R}^3 &\rightarrow S^3_{t_0}\subset\mathbb{R}^4\\ p=(\gamma,\theta,\phi) &\mapsto q_{t_0}=(x,y,z)=(\vec{r},u)\end{aligned}\tag{20}$$

where $\vec{r}:=(x,y,z):=(r\sin\phi\sin\theta,r\sin\phi\cos\theta,r\cos\phi)$ is the ordinary three-dimensional spatial vector, $r:=|\vec{r}|=t_0\sin\gamma$, and $u:=t_0\cos\gamma=t_0\sqrt{1-\sin^2\gamma}$ is the (fourth) dimension of the ambient or embedding space $\mathbb{R}^4$ where $S^3_{t_0}$ lives. It is also possible to define a two-dimensional vector $\vec{\ell}:=(x,y)\in S^1_\ell\subset\mathbb{R}^2$ such that $\ell:=|\vec{\ell}|=r\sin\phi$. Therefore, the three-component vector is now $\vec{r}=(\vec{\ell},z)\in S^2_r\subset\mathbb{R}^3$ and $z=r\cos\phi$ is the (third) extra dimension. Using these definitions, the first fundamental form of the sphere S^2_r and its linked infinitesimal distance are:

$$\begin{aligned}g_{S^2}&=\begin{pmatrix}r^2\sin^2\phi & 0\\ 0 & r^2\end{pmatrix}\ \Rightarrow\\ &\Rightarrow\ \mathrm{d}s^2_r:=(g_{S^2})_{\theta\theta}\mathrm{d}\theta^2+(g_{S^2})_{\phi\phi}\,\mathrm{d}\phi^2=r^2\sin^2\phi\,\mathrm{d}\theta^2+r^2\mathrm{d}\phi^2\ .\end{aligned}\tag{21}$$

Since $\ell=r\sin\phi$ and $\phi=\arcsin(\ell/r)$,

$$\mathrm{d}s^2_r:=(g_{S^2})_{\theta\theta}\,\mathrm{d}\theta^2+(g_{S^2})_{\phi\phi}\,\mathrm{d}\phi^2=\ell^2\mathrm{d}\theta^2+\frac{\mathrm{d}\ell^2}{1-\frac{\ell^2}{r^2}}.\tag{22}$$

Repeating the same process and since $\gamma=\arcsin(r/t_0)$, the distances over the hypersphere $S^3_{t_0}\subset\mathbb{R}^4$ are:

$$\mathrm{d}q^2_{t_0}=r^2\sin^2\phi\,\mathrm{d}\theta^2+r^2\mathrm{d}\phi^2+\frac{\mathrm{d}r^2}{1-\frac{r^2}{t_0^2}}\ =:\ r^2\mathrm{d}\Omega^2+\frac{\mathrm{d}r^2}{1-\frac{r^2}{t_0^2}}.\tag{23}$$

This is the metric for a **stationary hypersphere**. This metric can be directly obtained by taking the differential of equation (20)., for instance by taking the measures performed by an observer located at $o_{t_0}:=(\vec{0},t_0)\in S^3_{t_0}\subset\mathbb{R}^4$, that is:

$$\mathrm{d}(q_{t_0}-o_{t_0})^2=(\mathrm{d}\vec{r},\mathrm{d}u)^2=(\mathrm{d}\vec{r},\mathrm{d}u)^2=\left(\mathrm{d}\left(r\vec{e}_r\right),\mathrm{d}\left(t_0\sqrt{1-\sin^2\gamma}-t_0\right)\right)^2\tag{24}$$

where $\vec{e}_r:=\vec{r}/r$ is the unitary spatial vector. The last term contributes to:

$$\mathrm{d}u=\mathrm{d}\left(t_0\sqrt{1-\sin^2\gamma}\right)=-\frac{t_0\sin\gamma\cos\gamma\,\mathrm{d}\gamma}{\sqrt{1-\sin^2\gamma}}=-\frac{\mathrm{d}r}{\sqrt{1-\frac{r^2}{t_0^2}}}\frac{r}{t_0}\tag{25}$$

$$\mathrm{d}(q_{t_0}-o_{t_0})^2=\mathrm{d}u^2+\mathrm{d}r^2=\frac{\mathrm{d}r^2}{1-\frac{r^2}{t_0^2}}\frac{r^2}{t_0^2}+\mathrm{d}r^2=\frac{\mathrm{d}r^2}{1-\frac{r^2}{t_0^2}}\tag{26}$$

while $r\mathrm{d}\vec{e}_r$ contributes to $r^2\,\mathrm{d}\Omega^2$. Now, the FLRW metric for a linearly expanding hypersphere is easily obtained replacing the distance $r \to r' := (t_0/t)r$, that is $r'/t_0 = r/t$ and adding a scale factor $a(t) = t/t_0$ to the spatial distance, as well as adding the contribution of $\mathrm{d}t^2$:

$$\mathrm{d}s^2_{\mathrm{FLRW}} := \mathrm{d}t^2 - \mathrm{d}q^2_{\mathrm{FLRW}} = \mathrm{d}t^2 - \left(\frac{t}{t_0}\right)^2 \left(r'^2\mathrm{d}\Omega^2 + \frac{\mathrm{d}r'^2}{1-\frac{r'^2}{t_0^2}} \right). \tag{27}$$

However, the spatial term on the right is only valid assuming a static hypersphere. Therefore, one needs to repeat the calculus of equation (24), replacing $t_0 \to t$ and considering the contributions of $\mathrm{d}t$ within both $\mathrm{d}r$ and $\mathrm{d}u$ to obtain the distances over the hyperconical Universe with coordinates $s_{\mathcal{H}^4} = (t, r, \theta, \phi)$,

$$\mathrm{d}s^2_{\mathcal{H}^4} := \mathrm{d}t^2 - \mathrm{d}(q_t - o_t)^2 = \mathrm{d}t^2 \left(2\sqrt{1-\frac{r'^2}{t_0^2}} - 1 \right) - \frac{t^2}{t_0^2} \left(\frac{\mathrm{d}r'^2}{1-\frac{r'^2}{t_0^2}} + r'^2\mathrm{d}\Sigma^2 \right) - \frac{2r't}{t_0^2} \frac{\mathrm{d}r'\mathrm{d}t}{\sqrt{1-\frac{r'^2}{t_0^2}}} \tag{28}$$

where it has been used that $r = (t/t_0)r'$ to separate the contributions from $\mathrm{d}r^2$ to comoving spatial $\mathrm{d}r'^2$ and temporal $\mathrm{d}t^2$ terms. Now, by identifying the metric g in the distance $\mathrm{d}s^2_{\mathrm{Hyp}} = g_{\mathrm{tt}}\,\mathrm{d}t^2 - g_{r'r'}\,\mathrm{d}r'^2 - 2g_{r't}\,\mathrm{d}r'\mathrm{d}t$, lapse $g_{\mathrm{tt}} \neq 1$ and shift $g_{r't} \neq 0$ components emerge compared to the FLRW metric. Observe that the differential line $\mathrm{d}(s_{\mathcal{H}^4} - O_t)$ leads to a non-isometric embedding for the observers' path $O_t := (t, o_t) = (t, \vec{0}, t)$ because they measure distances from a set reference time, $O'_t := (t_0, \vec{0}, t)$ [6].

Nevertheless, the expansion terms of the metric g can be absorbed by a radially inhomogeneity in the purely spatial component, by changing the coordinate $t \to t' := t\sqrt{g_{\mathrm{tt}}}$. Thus, the metric expressed in the new coordinates differs little from the FLRW metric for $r' << t$,

$$g'_{\mathrm{tt}} = 1 \tag{29}$$

$$g'_{\phi\phi} = -a(t', r')^2 r'^2 sin^2\theta \tag{30}$$

$$g'_{\theta\theta} = -a(t', r')^2 r'^2 \tag{31}$$

$$\begin{aligned} g'_{r'r'} = g_{r'r'} - \frac{g^2_{0r}}{g_{00}} &= -a(t', r')^2 \frac{2 - \sqrt{1-\frac{r'^2}{t_0^2}}}{2\left(1-\frac{r'^2}{t_0^2}\right) - \sqrt{1-\frac{r'^2}{t_0^2}}} \\ &\approx -a(t', r')^2 \frac{1+\frac{r'^2}{2t_0^2}}{1-\frac{3r'^2}{2t_0^2}} \approx -a(t', r')^2 \left(1 + \frac{2r'^2}{t_0^2}\right) + \ldots \end{aligned} \tag{32}$$

with scale factor

$$a(t', r') = \frac{t'}{t_0\sqrt{2\left(\sqrt{1-\frac{r'^2}{t_0^2}} - 1\right) + 1}} \approx \frac{t'}{t_0\sqrt{1-\frac{r'^2}{t_0^2}}} \approx \frac{t'}{t_0}\left(1 + \frac{r'^2}{2t_0^2}\right). \tag{33}$$

In spite of the resemblance with a FLRW metric, the radial inhomogeneity leads to two remarkable features: (1) Local Ricci curvature of g is equivalent to a flat FLRW Universe with almost linear acceleration [6]. (2) Moreover, if g is projected over a plane, the inhomogeneity can be absorbed as a ΛCDM-like acceleration [22]. For instance, a possible family of projections could be the following:

Let $\gamma'(r') = \sin^{-1}(r'/t_0)$ be the coordinate angle, $\gamma'_k := \pi/3$ a constant corresponding to the real domain for the comoving distance r', and $\alpha \in \mathbb{R}_{\geq 0}$ be a fitting parameter. Now, we can define the family ${}_\sigma f^\alpha_{\hat{r}}(r') : \mathbb{R} \to \mathbb{R}$ of projections such that

$$ {}_\sigma f^\alpha_{\hat{r}}(r') := \sigma_\mathrm{t} t_0 \, \mathbf{trig}^{-1} \frac{\gamma'(r')}{\sigma_\mathrm{t}\left(1 - \frac{\gamma'(r')}{\gamma'_k}\right)^\alpha} \tag{34} $$

where **trig** is any trigonometric function that the first derivative is $\mathrm{trig}'(0) = 1$, mainly **sin**, **tan**, **sinh** and **tanh**, while $\sigma_\mathrm{t} \in \mathbb{C}$. For instance, [22] used **trig** = **tan** with two limit cases, ${}_\infty F_\gamma = \lim_{\sigma_\mathrm{t}\to\pm\infty} {}_\sigma f^\alpha_{\hat{r}}$, and ${}_2 f^\alpha_{\hat{r}} := \lim_{\sigma_\mathrm{t}\to\pm 2} {}_\sigma f^\alpha_{\hat{r}}$. Considering $k \equiv 1$ and $\Omega_r = 9.0 \pm 0.5 \cdot 10^{-5}$, their numerical solutions correspond to complex values:

$$ \alpha = 0.2830219501(1) \pm c_\alpha i \tag{35} $$

$$ \Omega_\Lambda = 0.6937181(17) \pm c_\omega $$

where the constants $c_\alpha, c_\omega \in \mathbb{R}$ become zero for $\sigma_\mathrm{t} = \pm 2.416\,113\,322(1)\,\mathrm{i}$. Nevertheless, as is discussed in this paper, the choice of projection family is not unique.

Appendix B. Example of estimation of main cosmological parameters using Maple

B.1. Basic definitions

Uploading Maple tools:

> *with*(*SolveTools*)

[*AbstractRootOfSolution*, *Basis*, *CancelInverses*, *Combine*, *Complexity*, *Engine*, *GreaterComplexity*, *Identity*, *Inequality*, *Linear*, *Parametric*, *Polynomial*, *PolynomialSystem*, *RationalCoefficients*, *SemiAlgebraic*, *SortByComplexity*]

Angle γ of an object with respect to an observer located at a spatial distance of r, assuming unitary age of the Universe, $t = 1$; and maximum value $\gamma_{\max}$ for which the (unprojected) hyperconical metric exists: [6, 22, 23]:

> $\gamma := r \to \arcsin(r)$

$$ \gamma := r \mapsto \arcsin(r) $$

> $\gamma_{\max} := \frac{2}{3}\pi$

$$ \gamma_{\max} = 2.094395103. $$

The auxiliary function $\xi(r)$ used in [6] to obtain the relationship between comoving distance and redshift:

> $\xi := r \to \mathrm{sqrt}(1 - (1 - \cos(\gamma(r)))^2)/(\cos(\gamma(r)) * (2 * (\cos(\gamma(r)) - 1) + 1))$

$$ \xi = x \mapsto \frac{\sqrt{1-(1-\cos(\gamma(r)))^2}}{\cos(\gamma(r))\cdot(2\cdot\cos(\gamma(r))-1)} $$

> $\xi_{\mathrm{tayl}} := r \to \mathrm{taylor}(\xi(r), r = 0, 10)$

$$ \xi_{\mathrm{tayl}} := r \mapsto \mathrm{taylor}(\xi(r), r = 0, 10). $$

Solving the comoving distance r_z as a function of redshift (z):

> $r_z := \text{solve}\left(\int \xi_{\text{tayl}}(r)\mathrm{d}x = \log(1+z), x\right)$

$$r_z := z - \tfrac{1}{2}z^2 - \tfrac{1}{6}z^3 + \tfrac{1}{2}z^4 - \tfrac{13}{40}z^5 + \mathrm{O}\left(z^6\right)$$

B.2. Definition of families of projections under the global and local approaches

B.2.1. The global approach with two parameters $\alpha \in (0,1]$ and $\gamma_0 \in \mathbb{R}$

> $f_{\text{glob}} := r \to r \cdot \left(\dfrac{2-\cos(\gamma(r))}{1-\frac{\gamma(r)}{\gamma_0}}\right)^{\alpha}$

$$f_{\text{glob}} := r \mapsto r \cdot \left(\tfrac{2-\cos(\gamma(x))}{1-\frac{g(r)}{\gamma_0}}\right)^{\alpha}.$$

Local approach, with three or more parameters $(\alpha, b_1, b_2, \ldots)$,$\alpha \in (0,1]$, $b_i \in (0,1)$:

> $f_{\text{loc}} := r \to r \cdot \left(\dfrac{2}{1+(1-b_1\cdot x + b_2 \cdot r^2)\cdot\cos(\gamma(r))}\right)^{a}.$

Although the set of three parameters (α, b_1, b_2) is enough to find the local solution, two more terms (b_3 and b_4) are considered to check consistency of the higher-order equations:

> $f_{\text{loc}} := r \to x \cdot \left(\dfrac{2}{1+(1-b_1\cdot x + b_2 \cdot r^2 + b_3\cdot x^3 + b_4 \cdot x^4)\cdot\cos(\gamma(r))}\right)^{a}$

$$f_{\text{loc}} := r \mapsto r \cdot \left(\frac{2}{1+(1-b_1\cdot x + b_2 \cdot x^2 + b_3\cdot r^3 + b_4 \cdot x^4)\cdot\cos(\gamma(x))}\right)^{a}.$$

To ensure local consistency (equation (8)), it is necessary to set that

> $b_1 := 1$

$$b_1 := 1.$$

B.3. Equivalent Hubble parameter obtained from the hyperconical model

B.3.1. Under the global approach

> $H_{\text{glob}} := \text{simplify}\left(\text{series}\left(\left(\dfrac{\mathrm{d}}{\mathrm{d}z} f_{\text{glob}}(r_z)\right)^{-1}, z=0,5\right)\right)$

$$\begin{aligned} H_{\text{glob}} = 1 &+ \frac{-2a+\gamma_0}{\gamma_0} z + \frac{1}{2}\frac{(-3a+3)\,{\gamma_0}^2 - 2a\gamma_0 + 5\,\alpha^2 - 3a}{{\gamma_0}^2} z^2 \\ &- \frac{1}{3}\frac{a\left(-12\,\alpha\,{\gamma_0}^2 + 8\,\alpha^2 + 7\,{\gamma_0}^2 - 12a + 4\right)}{{\gamma_0}^3} z^3 \\ &+ \frac{1}{24}\frac{\begin{array}{c} 65\,\alpha^4 + \left(-162\,{\gamma_0}^2 + 32\,\gamma_0 - 162\right)\alpha^3 + \left(39\,{\gamma_0}^4 - 48\,{\gamma_0}^3 + 147\,{\gamma_0}^2\right. \\ \left. -48\,\gamma_0 + 127\right)\alpha^2 + \left(-15\,{\gamma_0}^4 + 28\,{\gamma_0}^3 - 35\,{\gamma_0}^2 + 16\,\gamma_0 - 30\right)\alpha + 9\,{\gamma_0}^4 \end{array}}{{\gamma_0}^4} z^4 + \mathrm{O}\left(z^5\right) \end{aligned}$$

> $H^j_{\text{glob}} := \text{eval}\left(\dfrac{1}{j!}\dfrac{\mathrm{d}^j}{\mathrm{d}z^j} H_{\text{glob}}, z=0\right).$

B.3.2. Under the local approach

> $H_{\rm loc} := \mathrm{simplify}(\mathrm{series}((\frac{\mathrm{d}}{\mathrm{d}z} f_{\rm loc}(r_z))^{-1}, z=0,5))$

$$H_{\rm loc} := 1+(-\alpha+1)z+\left(\frac{3}{2}+\frac{5\,\alpha^2}{8}+\frac{(12\,b_2-13)\,\alpha}{8}\right)z^2-\frac{1}{6}\alpha\left(2\,\alpha^2+12\,\alpha b_2-9\,\alpha-6\,b_2-12\,b_3+3\right)z^3$$
$$+\left(\frac{3}{8}+\frac{65\,\alpha^4}{384}+\frac{(648\,b_2-422)\,\alpha^3}{384}+\frac{\left(624\,{b_2}^2-1080\,b_2-1056\,b_3-13\right)\alpha^2}{384}\right.$$
$$\left.+\frac{\left(-240\,{b_2}^2+48\,b_2+96\,b_3+960\,b_4-174\right)\alpha}{384}\right)z^4+\mathrm{O}\left(z^5\right)$$

> $H^j_{\rm loc} := \mathrm{eval}\left(\frac{1}{j!}\frac{\mathrm{d}^j}{\mathrm{d}z^j} H_{\rm loc}, z=0\right).$

B.3.3. Standard Hubble parameter and its Taylor-Maclaurin expansion

$H := z \to \mathrm{sqrt}(\Omega_r\cdot(1+z)^4+\Omega_m\cdot(1+z)^3+\Omega_K\cdot(1+z)^2+\Omega_\Lambda)$

$$H = z \mapsto \sqrt{\Omega_r\cdot(z+1)^4+\Omega_m\cdot(z+1)^3+\Omega_K\cdot(z+1)^2+\Omega_\Lambda}$$

> $H_{\rm stan} := \mathrm{simplify}(\mathrm{taylor}(H(z), z=0,5))$

$$H_{\rm stan}: = \sqrt{\Omega_r+\Omega_m+\Omega_K+\Omega_\Lambda}+\frac{1}{2}\frac{4\,\Omega_r+3\,\Omega_m+2\,\Omega_K}{\sqrt{\Omega_r+\Omega_m+\Omega_K+\Omega_\Lambda}}z$$
$$+\frac{1}{2}\frac{\frac{3\,{\Omega_m}^2}{4}+(\Omega_K+3\,\Omega_\Lambda+3\,\Omega_r)\,\Omega_m+2\,{\Omega_r}^2+(3\,\Omega_K+6\,\Omega_\Lambda)\,\Omega_r+\Omega_K\Omega_\Lambda}{(\Omega_r+\Omega_m+\Omega_K+\Omega_\Lambda)^{\frac{3}{2}}}z^2$$
$$+\frac{\begin{array}{l}-{\Omega_m}^3+(-2\,\Omega_K-20\,\Omega_\Lambda)\,{\Omega_m}^2+((-20\,\Omega_\Lambda+4\,\Omega_r)\,\Omega_K+8\,\Omega_\Lambda\,(\Omega_\Lambda-5\,\Omega_r))\,\Omega_m\\ \quad -8\,(\Omega_\Lambda-\Omega_r)\left({\Omega_K}^2-4\,\Omega_\Lambda\Omega_r\right)\end{array}}{16\,(\Omega_r+\Omega_m+\Omega_K+\Omega_\Lambda)^{\frac{5}{2}}}z^3$$
$$+\frac{64\,{\Omega_\Lambda}^3\Omega_r-\left(240\,{\Omega_m}^2+(160\,\Omega_K+896\,\Omega_r)\,\Omega_m+16\,{\Omega_K}^2+256\,\Omega_r\Omega_K+896\,{\Omega_r}^2\right){\Omega_\Lambda}^2}{128\,(\Omega_r+\Omega_m+\Omega_K+\Omega_\Lambda)^{\frac{7}{2}}}z^4$$
$$+\frac{\begin{array}{l}\left(168\,{\Omega_m}^3+(280\,\Omega_K+560\,\Omega_r)\,{\Omega_m}^2+\left(224\,{\Omega_K}^2+448\,\Omega_r\Omega_K+640\,{\Omega_r}^2\right)\Omega_m\right.\\ \left.\quad +64\,{\Omega_K}^3+224\,{\Omega_K}^2\Omega_r+320\,{\Omega_r}^3\right)\Omega_\Lambda\end{array}}{128\,(\Omega_r+\Omega_m+\Omega_K+\Omega_\Lambda)^{\frac{7}{2}}}z^4$$
$$-\frac{32\,\left(\frac{3\,{\Omega_m}^2}{8}+(\Omega_K+\Omega_r)\,\Omega_m+\frac{5\,\Omega_r\Omega_K}{2}\right)\left(\Omega_r\Omega_K-\frac{{\Omega_m}^2}{4}\right)}{128\,(\Omega_r+\Omega_m+\Omega_K+\Omega_\Lambda)^{\frac{7}{2}}}z^4+\mathrm{O}\left(z^5\right)$$

> $H^j_{\rm stan} := \mathrm{eval}\left(\frac{1}{j!}\frac{\mathrm{d}^j}{\mathrm{d}z^j} H_{\rm stan}, z=0\right).$

B.4. Equalising for each approach order of the Hubble parameter

B.4.1. Systems of the 2nd-, 3rd- and 4th-order equations for $H_{\rm glob} = H_{\rm stan}$

> $GSys2 := \{H^0_{\rm stan} = H^0_{\rm glob}, H^1_{\rm stan} = H^1_{\rm glob}, H^2_{\rm stan} = H^2_{\rm glob}\}$

$$GSys2 = \left\{ \sqrt{\Omega_r+\Omega_m+\Omega_K+\Omega_\Lambda} = 1, \frac{4\,\Omega_r+3\,\Omega_m+2\,\Omega_K}{2\,\sqrt{\Omega_r+\Omega_m+\Omega_K+\Omega_\Lambda}} = \frac{-2\,\alpha+\gamma_0}{\gamma_0}\,, \right.$$
$$\frac{\frac{3\,{\Omega_m}^2}{4}+(\Omega_K+3\,\Omega_\Lambda+3\,\Omega_r)\,\Omega_m+2\,{\Omega_r}^2+(3\,\Omega_K+6\,\Omega_\Lambda)\,\Omega_r+\Omega_K\Omega_\Lambda}{2\,(\Omega_r+\Omega_m+\Omega_K+\Omega_\Lambda)^{\frac{3}{2}}}$$
$$\left. = \frac{(-3\,\alpha+3)\,{\gamma_0}^2-2\,\alpha\gamma_0+5\,\alpha^2-3a}{2\,{\gamma_0}^2} \right\}$$

> $GSys3 := \{H^0_{\rm stan} = H^0_{\rm glob}, H^1_{\rm stan} = H^1_{\rm glob}, H^2_{\rm stan} = H^2_{\rm glob}, H^3_{\rm stan} = H^3_{\rm glob}\}$

$$GSys3 := \left\{ \sqrt{\Omega_r+\Omega_m+\Omega_K+\Omega_\Lambda} = 1, \frac{4\,\Omega_r+3\,\Omega_m+2\,\Omega_K}{2\,\sqrt{\Omega_r+\Omega_m+\Omega_K+\Omega_\Lambda}} = \frac{-2\,\alpha+\gamma_0}{\gamma_0}, \right.$$
$$\frac{-{\Omega_m}^3+(-2\,\Omega_K-20\,\Omega_\Lambda)\,{\Omega_m}^2+((-20\,\Omega_\Lambda+4\,\Omega_r)\,\Omega_K+8\,\Omega_\Lambda\,(\Omega_\Lambda-5\,\Omega_r))\,\Omega_m}{16\,(\Omega_r+\Omega_m+\Omega_K+\Omega_\Lambda)^{\frac{5}{2}}}$$
$$\frac{-8\,(\Omega_\Lambda-\Omega_r)\left({\Omega_K}^2-4\,\Omega_\Lambda\Omega_r\right)}{16\,(\Omega_r+\Omega_m+\Omega_K+\Omega_\Lambda)^{\frac{5}{2}}}$$
$$= -\frac{a\left(-12\,\alpha{\gamma_0}^2+8\,\alpha^2+7\,{\gamma_0}^2-12\,\alpha+4\right)}{3\,{\gamma_0}^3},$$
$$\frac{\frac{3\,{\Omega_m}^2}{4}+(\Omega_K+3\,\Omega_\Lambda+3\,\Omega_r)\,\Omega_m+2\,{\Omega_r}^2+(3\,\Omega_K+6\,\Omega_\Lambda)\,\Omega_r+\Omega_K\Omega_\Lambda}{2\,(\Omega_r+\Omega_m+\Omega_K+\Omega_\Lambda)^{\frac{3}{2}}}$$
$$\left. = \frac{(-3\,\alpha+3)\,{\gamma_0}^2-2\,\alpha\gamma_0+5\,\alpha^2-3a}{2\,{\gamma_0}^2} \right\}$$

> $GSys4 := \{H^0_{\rm stan} = 1, H^1_{\rm stan} = H^1_{\rm glob}, H^2_{\rm stan} = H^2_{\rm glob}, H^3_{\rm stan} = H^3_{\rm glob}, H^4_{\rm stan} = H^4_{\rm glob}\}$

$$GSys4 := \left\{ \sqrt{\Omega_r+\Omega_m+\Omega_K+\Omega_\Lambda} = 1, \frac{4\,\Omega_r+3\,\Omega_m+2\,\Omega_K}{2\,\sqrt{\Omega_r+\Omega_m+\Omega_K+\Omega_\Lambda}} = \frac{-2\,\alpha+\gamma_0}{\gamma_0}, \right.$$
$$\times \frac{-{\Omega_m}^3+(-2\,\Omega_K-20\,\Omega_\Lambda)\,{\Omega_m}^2+((-20\,\Omega_\Lambda+4\,\Omega_r)\,\Omega_K+8\,\Omega_\Lambda\,(\Omega_\Lambda-5\,\Omega_r))\,\Omega_m}{16\,(\Omega_r+\Omega_m+\Omega_K+\Omega_\Lambda)^{\frac{5}{2}}}$$
$$\frac{-8\,(\Omega_\Lambda-\Omega_r)\left({\Omega_K}^2-4\,\Omega_\Lambda\Omega_r\right)}{16\,(\Omega_r+\Omega_m+\Omega_K+\Omega_\Lambda)^{\frac{5}{2}}}$$
$$= -\frac{a\left(-12\,\alpha{\gamma_0}^2+8\,\alpha^2+7\,{\gamma_0}^2-12\,\alpha+4\right)}{3\,{\gamma_0}^3},$$
$$\times \frac{1}{128}\,\frac{64\,{\Omega_\Lambda}^3\Omega_r+\left(-240\,{\Omega_m}^2+(-160\,\Omega_K-896\,\Omega_r)\,\Omega_m-16\,{\Omega_K}^2\right.}{(\Omega_r+\Omega_m+\Omega_K+\Omega_\Lambda)^{\frac{7}{2}}}$$
$$\left.\frac{-256\,\Omega_r\Omega_K-896\,{\Omega_r}^2)\,{\Omega_\Lambda}^2}{(\Omega_r+\Omega_m+\Omega_K+\Omega_\Lambda)^{\frac{7}{2}}}\right. z^4$$
$$+\frac{1}{128}\,\frac{\left(168\,{\Omega_m}^3+(280\,\Omega_K+560\,\Omega_r)\,{\Omega_m}^2+\left(224\,{\Omega_K}^2+448\,\Omega_r\Omega_K+640\,{\Omega_r}^2\right)\Omega_m\right.}{(\Omega_r+\Omega_m+\Omega_K+\Omega_\Lambda)^{\frac{7}{2}}}$$
$$\left.\frac{+64\,{\Omega_K}^3+224\,{\Omega_K}^2\Omega_r+320\,{\Omega_r}^3)\,\Omega_\Lambda}{(\Omega_r+\Omega_m+\Omega_K+\Omega_\Lambda)^{\frac{7}{2}}}\right. z^4$$
$$-\frac{1}{128}\,\frac{32\,\left(\frac{3\,{\Omega_m}^2}{8}+(\Omega_K+\Omega_r)\,\Omega_m+\frac{5\,\Omega_r\Omega_K}{2}\right)\left(\Omega_r\Omega_K-\frac{{\Omega_m}^2}{4}\right)}{(\Omega_r+\Omega_m+\Omega_K+\Omega_\Lambda)^{\frac{7}{2}}}$$

$$
\begin{aligned}
&65\,\alpha^4+\left(-162\,{\gamma_0}^2+32\,\gamma_0-162\right)\alpha^3+\left(39\,{\gamma_0}^4-48\,{\gamma_0}^3+147\,{\gamma_0}^2-48\,\gamma_0+127\right)\alpha^2\\
&\quad+\left(-15\,{\gamma_0}^4+28\,{\gamma_0}^3-35\,{\gamma_0}^2+16\,\gamma_0-30\right)\alpha+9\,{\gamma_0}^4\\
&=\frac{}{24\,{\gamma_0}^4},\\
&\times\frac{\frac{3\,{\Omega_m}^2}{4}+\left(\Omega_K+3\,\Omega_\Lambda+3\,\Omega_r\right)\Omega_m+2\,{\Omega_r}^2+\left(3\,\Omega_K+6\,\Omega_\Lambda\right)\Omega_r+\Omega_K\Omega_\Lambda}{2\,\left(\Omega_r+\Omega_m+\Omega_K+\Omega_\Lambda\right)^{\frac{3}{2}}}\\
&=\frac{(-3\,\alpha+3)\,{\gamma_0}^2-2\,\alpha\gamma_0+5\,\alpha^2-3a}{2\,{\gamma_0}^2}\Bigg\}
\end{aligned}
$$

B.4.2. Systems of the 2nd-, 3rd- and 4th-order equations for $H_{\rm loc}=H_{\rm stan}$

> $LSys1:=\{H^0_{\rm stan}=H^0_{\rm loc},H^1_{\rm stan}=H^1_{\rm loc}\}$

$$LSys1:=\left\{\sqrt{\Omega_r+\Omega_m+\Omega_K+\Omega_\Lambda}=1,\frac{4\,\Omega_r+3\,\Omega_m+2\,\Omega_K}{2\,\sqrt{\Omega_r+\Omega_m+\Omega_K+\Omega_\Lambda}}=-a+1\right\}$$

> $LSys2:=\{H^0_{\rm stan}=H^0_{\rm loc},H^1_{\rm stan}=H^1_{\rm loc},H^2_{\rm stan}=H^2_{\rm loc}\}$

$$
\begin{aligned}
LSys2:=&\left\{\sqrt{\Omega_r+\Omega_m+\Omega_K+\Omega_\Lambda}=1,\right.\\
&\frac{\frac{3\,{\Omega_m}^2}{4}+\left(\Omega_K+3\,\Omega_\Lambda+3\,\Omega_r\right)\Omega_m+2\,{\Omega_r}^2+\left(3\,\Omega_K+6\,\Omega_\Lambda\right)\Omega_r+\Omega_K\Omega_\Lambda}{2\,\left(\Omega_r+\Omega_m+\Omega_K+\Omega_\Lambda\right)^{\frac{3}{2}}}\\
&=\frac{3}{2}+\frac{5\,\alpha^2}{8}+\frac{(12\,b_2-13)\,a}{8},\\
&\left.\frac{4\,\Omega_r+3\,\Omega_m+2\,\Omega_K}{2\,\sqrt{\Omega_r+\Omega_m+\Omega_K+\Omega_\Lambda}}=-a+1\right\}
\end{aligned}
$$

> $LSysN:=\{H^0_{\rm stan}=H^0_{\rm loc},H^1_{\rm stan}=H^1_{\rm loc},H^2_{\rm stan}=H^2_{\rm loc},\ldots,H^N_{\rm stan}=H^N_{\rm loc}\}$

$$
\begin{aligned}
LSysN:=&\left\{\sqrt{\Omega_r+\Omega_m+\Omega_K+\Omega_\Lambda}=1,\right.\\
&\frac{\frac{3\,{\Omega_m}^2}{4}+\left(\Omega_K+3\,\Omega_\Lambda+3\,\Omega_r\right)\Omega_m+2\,{\Omega_r}^2+\left(3\,\Omega_K+6\,\Omega_\Lambda\right)\Omega_r+\Omega_K\Omega_\Lambda}{2\,\left(\Omega_r+\Omega_m+\Omega_K+\Omega_\Lambda\right)^{\frac{3}{2}}}\\
&=\frac{3}{2}+\frac{5\,\alpha^2}{8}+\frac{(12\,b_2-13)\,a}{8},\\
&\left.\frac{4\,\Omega_r+3\,\Omega_m+2\,\Omega_K}{2\,\sqrt{\Omega_r+\Omega_m+\Omega_K+\Omega_\Lambda}}=-a+1,\ldots\right\}
\end{aligned}
$$

B.5. Some explicit solutions

B.5.1. Under the global approach with $\Omega_r = 0$

> SolGSys2a := solve(eval($GSys2, \Omega_r = 0$), $\{\Omega_K, \Omega_m, \Omega_\Lambda\}$)

$$\text{SolGSys2a} := \left\{ \Omega_K = -\frac{-3\ \alpha {\gamma_0}^2 + 9\ \alpha^2 - 2\ \alpha\gamma_0 + 2\ {\gamma_0}^2 - 3a}{{\gamma_0}^2}\ , \right.$$
$$\Omega_\Lambda = \frac{-3\ \alpha {\gamma_0}^2 + 9\ \alpha^2 + 2\ \alpha\gamma_0 + 3\ {\gamma_0}^2 - 3a}{3\ {\gamma_0}^2},$$
$$\left. \Omega_m = \frac{2\ \left(-3\ \alpha {\gamma_0}^2 + 9\ \alpha^2 - 4\ \alpha\gamma_0 + 3\ {\gamma_0}^2 - 3\ \alpha\right)}{3\ {\gamma_0}^2} \right\}$$

B.5.2. Under the global approach with $\Omega_r = 0$ and $\epsilon = 0$

> $SolGSys2b := solve(eval(eval(eval(GSys2, \Omega_r = 0), \alpha = \frac{\gamma_0 \cdot 5}{18} \cdot (1+0)), \gamma_0 = 2 \cdot (1+\delta)), \{\Omega_K, \Omega_m, \Omega_\Lambda\})$

$$\text{SolGSys2b} := \left\{ \Omega_K = \frac{60\ \delta^2 + 43\ \delta - 2}{36\ (1+\delta)}, \Omega_\Lambda = -\frac{20\ \delta^2 - 11\ \delta - 26}{36\ (1+\delta)}\ , \right.$$
$$\left. \Omega_m = -\frac{20\ \delta^2 + 9\ \delta - 6}{18\ (1+\delta)} \right\}$$

B.5.3. Under the global approach with $\epsilon = 0$

> SolGSys2c := solve(eval(eval($GSys2, \alpha = \frac{\gamma_0 \cdot 5}{18} \cdot (1+0)), \gamma_0 = 2 \cdot (1+\delta)), \{\Omega_K, \Omega_m, \Omega_\Lambda\})$

$$\text{SolGSys2c} := \left\{ \Omega_K = \frac{72\ \Omega_r\delta + 60\ \delta^2 + 72\ \Omega_r + 43\ \delta - 2}{36\ (1+\delta)}\ , \Omega_\Lambda = -\frac{12\ \Omega_r\delta + 20\ \delta^2 + 12\ \Omega_r - 11\ \delta - 26}{36\ (1+\delta)}, \right.$$
$$\left. \Omega_m = -\frac{48\ \Omega_r\delta + 20\ \delta^2 + 48\ \Omega_r + 9\ \delta - 6}{18\ (1+\delta)} \right\}$$

B.5.4. Under the local approach with $\Omega_r = 0$

> SolLSys2 :=
eval(eval(eval(solve($Sys2, \{\Omega_r, \Omega_m, \Omega_\Lambda\}), \Omega_r = 0), \Omega_K = 0), $b_2 = -0.6250\ 000\ 000$)

$$\text{SolLSys2} := \left\{ 0 = \tfrac{9}{8}\alpha^2 - 2.562\,500\,00\,00\ \alpha + 1, \Omega_\Lambda = \tfrac{2}{3} + \tfrac{3}{8}\alpha^2 - 0.187\,500\,00\,00\ \alpha, \right.$$
$$\left. \Omega_m = -\tfrac{2}{3} - \tfrac{3}{2}\alpha^2 + 2.750\,000\,00\,00\ \alpha \right\}$$

B.6. Some numerical solutions

B.6.1. Under the 2rd-order global approach with $\Omega_K := 0$, $\Omega_r \approx 0$ and $\delta := \frac{\pi}{3} - 1$

> Glob2a := solve(eval(eval(eval($GSys2, \Omega_K = 0), \gamma_0 = \gamma_{\max}), \Omega_r = 0), $\{\alpha, \Omega_m, \Omega_\Lambda\}$)

Glob2a := $\big(\{\Omega_\Lambda = 0.702\,482\,1736, \Omega_m = 0.297\,517\,8264, \alpha = 0.579\,857\,6424\}$,
$\{\Omega_\Lambda = 1.403\,529\,648, \Omega_m = -0.403\,529\,6479, \alpha = 1.681\,060\,440\}\big)$

% Rejected by $|\epsilon| > 0.05$ against the hypothesised.

B.6.2. Under the 2rd-order global approach with $\Omega_K \approx 0$, $\Omega_r \approx (9.0 \pm 0.5) \cdot 10^{-5}$ *and* $\delta := \frac{\pi}{3} - 1$

> $Glob2b := \text{solve}(\text{eval}(\text{eval}(\text{eval}(\text{eval}(GSys2, \alpha = \frac{\gamma_{\max} \cdot 5}{18} \cdot (1+\epsilon)), \Omega_K = 0), \gamma_0 = \gamma_{\max}), \Omega_r = (9.0 \pm 0.5) \cdot 10^{-5}), \{\epsilon, \Omega_m, \Omega_\Lambda\})$

$Glob2b := \big(\{\Omega_\Lambda = 0.70246\,03068, \Omega_m = 0.29\,744\,46\,832, \epsilon = -0.00\,344\,2680\,711\},$
$\{\Omega_\Lambda = 1.40\,361\,4854, \Omega_m = -0.40\,370\,98\,636, \epsilon = 1.88\,967\,4596\}\big)$ % Rejected by $|\epsilon| > 0.05$ against the hypothesised.

B.6.3. Under the 2nd-order global approach with $\epsilon = 0 = \delta$

> $Glob2c := \text{solve}(\text{eval}(\text{eval}(\text{eval}(GSys2, \alpha = \frac{2 \cdot 5}{18}), \gamma_0 = 2), \Omega_r < 10^{-6}, \{\Omega_K, \Omega_m, \Omega_\Lambda\})$

$Glob2c := \big(\{\Omega_K = -0.05\,555\,365\,536, \Omega_\Lambda = 0.72\,222\,19\,055, \Omega_m = 0.33\,333\,07\,997\}\big).$

B.6.4. Under the 3rd-order global approach with $\delta := \frac{\pi}{3} - 1$

> $Glob3a := \text{solve}(\text{eval}(\text{eval}(\text{eval}(GSys3, \alpha = \frac{\gamma_{\max} \cdot 5}{18} \cdot (1+\epsilon)), \Omega_r = (9.0 \pm 0.5) \cdot 10^{-5}), \gamma_0 = \gamma_{\max}), \{\Omega_m, \Omega_\Lambda, \epsilon, \Omega_K\})$

$Glob3a := \big(\{\Omega_K = -0.01\,506\,989\,666, \Omega_\Lambda = 0.70\,326\,45\,994, \Omega_m = 0.31\,171\,52\,973, \epsilon = -0.01\,482\,948\,873\},$
$\{\Omega_K = -1.03\,749\,9098, \Omega_\Lambda = 0.82\,629\,53\,330, \Omega_m = 1.21\,111\,3765, \epsilon = -0.60\,283\,2789\},$
% Rejected by $|\epsilon| > 0.05$ against the hypothesised
$\{\Omega_K = -23.00\,134\,246, \Omega_\Lambda = 10.88\,033\,003, \Omega_m = 13.12\,092\,243, \epsilon = 6.77\,560\,1874\}\big)$
% Rejected by $|\epsilon| > 0.05$ against the hypothesised.

B.6.5. Under the 3rd-order global approach with $\delta := 0$

> $Glob3b := \text{solve}(\text{eval}(\text{eval}(\text{eval}(GSys3, \gamma_0 = 2 \cdot (1+\epsilon)), \alpha = \frac{5}{18} \cdot 2 \cdot (1+\epsilon), \Omega_r = (9.0 \pm 0.5) \cdot 10^{-5}), \{\Omega_m, \Omega_\Lambda, \epsilon, \Omega_K\})$

$Glob3b := \big(\{\Omega_K = -0.01\,180\,432\,187, \Omega_\Lambda = 0.70\,767\,01\,777, \Omega_m = 0.30\,403\,90\,442,$
$\epsilon = 0.03\,446\,605\,021\big\},$
$\{\Omega_K = -1.77\,716\,3130 - 0.67\,695\,11\,395\text{I}, \Omega_\Lambda = 1.29\,612\,3114 + 0.22\,565\,03\,798\text{I},$
$\Omega_m = 1.48\,094\,4916 + 0.45\,130\,07\,597\text{I}, \epsilon = -0.93\,307\,67\,129 + 0.32\,720\,25\,928\text{I}\},$
% *Rejected by* $|\epsilon| > 0.05$ *against the hypothesised*
$\{\Omega_K = -1.77\,716\,3130 + 0.67\,695\,11\,395\text{I}, \Omega_\Lambda = 1.29\,612\,3114 - 0.22\,565\,03\,798\text{I},$
$\Omega_m = 1.48\,094\,4916 - 0.45\,130\,07\,597\text{I}, \epsilon = -0.93\,307\,67\,129 - 0.32\,720\,25\,928\text{I}\}\big)$
% *Rejected by* $|\epsilon| > 0.05$ *against the hypothesised*

> $\alpha_0 := \frac{5}{18} \cdot 2 \cdot (1 + 0.0344660502)$

$\alpha_0 := 0.57\,470\,33\,611$

B.6.6. Under the 3rd-order global approach with $\delta \approx \epsilon$

> $Glob3c := solve(eval(eval(eval(eval(GSys3, \gamma_0 = 2\cdot(1+\epsilon)), \alpha = \frac{5}{18}\cdot 2\cdot(1+\epsilon)^2), \Omega_r = (9.0\pm 0.5)\cdot 10^{-5}), \{\Omega_m, \Omega_\Lambda, \epsilon, \Omega_K\})$

$$Glob3c := \big(\{\Omega_K = -0.00822461858\,7, \Omega_\Lambda = 0.71341027\,73, \Omega_m = 0.29471934\,13, \epsilon = 0.01872009\,185\},$$
$$\{\Omega_K = -0.83143067\,45, \Omega_\Lambda = 0.16225649\,48, \Omega_m = 1.66907918\,0, \epsilon = -2.21028057\},$$
$$\%\ \textit{Rejected by}\ |\epsilon| > 0.05\ \textit{against the hypothesised}$$
$$\{\Omega_K = -1.49450\,5474 + 0.20030\,60777\,\mathrm{I}, \Omega_\Lambda = 0.89976\,89646 + 0.01441\,767501\,\mathrm{I}, \Omega_m = 1.59464\,1509 - 0.21472\,37527\,\mathrm{I}, \epsilon = -0.81\,57642\,221 + 0.21\,92031\,925\mathrm{I}\},$$
$$\%\ \textit{Rejected by}\ |\epsilon| > 0.05\ \textit{against the hypothesised}$$
$$\{\Omega_K = -1.49450\,5474 - 0.20030\,60777\,\mathrm{I}, \Omega_\Lambda = 0.89976\,89646 - 0.01441\,767501\,\mathrm{I}, \Omega_m = 1.59464\,1509 + 0.21472\,37527\,\mathrm{I}, \epsilon = -0.81\,57642\,221 - 0.21\,92031\,925\mathrm{I}\}\big)\ \%\ \textit{Rejected by}\ |\epsilon| > 0.05\ \textit{against the hypothesised}$$

B.6.7. Under the local approach with $\Omega_K := 0$*, for the second-, third- and fourth-order expansions*

> $Loc2 := \mathrm{solve}(\mathrm{eval}(\mathrm{eval}(\mathrm{eval}(\mathrm{eval}(LSys2, j = 0), \Omega_K = 0), \alpha = 0.5), \Omega_r = 0.0), \{b_2, \Omega_m, \Omega_\Lambda\})$

$$Loc2 := \{\Omega_\Lambda = 0.66666\,63333, \Omega_m = 0.33333\,26667, b_2 = -0.62500\,06667\}$$

> $Loc3 := \mathrm{solve}(\mathrm{eval}(\mathrm{eval}(\mathrm{eval}(LSys3, \Omega_r = 0.0), \alpha = 0.5), \Omega_K = 0), \{b_2, \Omega_\Lambda, \Omega_m, b_3\})$

$$Loc3 := \{\Omega_\Lambda = 0.66666\,66667, \Omega_m = 0.33333\,33333, b_2 = -0.62500\,00000, b_3 = -0.10416\,66667\}$$

> $Loc4 := \mathrm{solve}(\mathrm{eval}(\mathrm{eval}(\mathrm{eval}(LSys4, \Omega_r = 0.0), \alpha = 0.5), \Omega_K = 0), \{b_2, \Omega_\Lambda, \Omega_m, b_3, b_4\})$

$$Loc4 := \{\Omega_\Lambda = 0.66666\,66667, \Omega_m = 0.33333\,33333, b_2 = -0.62500\,00000, b_3 = -0.10416\,66667, b_4 = -0.34947\,91666\}.$$

ORCID iDs

Robert Monjo https://orcid.org/0000-0003-3100-2394
Rutwig Campoamor-Stursberg https://orcid.org/0000-0003-2907-8533

References

[1] Riess A G, Casertano S, Yuan W, Macri L M and Scolnic D 2019 Large Magellanic Cloud cepheid standards provide a 1% foundation for the determination of the Hubble constant and stronger evidence for physics beyond ΛCDM *Astrophys. J.* **876** 85
[2] Riess A G, Casertano S, Yuan W Bowers J B, Macri L, Zinn J C and Scolnic D 2021 Cosmic distances calibrated to 1% precision with gaia EDR3 parallaxes and Hubble space telescope photometry of 75 milky way cepheids confirm tension with ΛCDM *Astrophys. J. Lett.* **908** L6
[3] Riess A G *et al* 2022 Comprehensive measurement of the local value of the Hubble constant with 1 km s^{-1} Mpc^{-1} uncertainty from the Hubble space telescope and the SH0ES team *Astrophys. J. Lett.* **934** L7
[4] Aghanim N *et al* (Planck Collaboration) 2020 Planck 2018 results. VI. Cosmological parameters *Astron. Astrophys.* **641** A6

[5] Di Valentino E, Mena O, Pan S, Visinell L, Yang W, Melchiorri A, Mota D F Riess A G and Silk J 2021 In the realm of the Hubble tension -a review of solutions *Class. Quantum Grav.* **38** 153001
[6] Monjo R 2017 Study of the observational compatibility of an inhomogeneous cosmology with linear expansion according to SNe Ia *Phys. Rev.* D **96** 103505
[7] Camarena D Marra V, Sakr Z and Clarkson C 2022 A void in the Hubble tension? The end of the line for the Hubble bubble *Class. Quantum Grav.* **39** 184001
[8] Poulin V, Smith T L, Grin D, Karwal T and Kamionkowski M 2018 Cosmological implications of ultralight axionlike fields *Phys. Rev.* D **98** 083525
[9] Poulin V, Smith T L, Karwal T and Kamionkowski M 2019 Early dark energy can resolve the Hubble tension *Phys. Rev. Lett.* **122** 221301
[10] Kamionkowski M and Riess A G 2022 The Hubble tension and early dark energy (arXiv:2211.04492)
[11] Herold L, Ferreira E G M and Komatsu E 2022 New constraint on early dark energy from planck and boss data using the profile likelihood *Astrophys. J. Lett.* **929** L16
[12] Gurzadyan V G and Stepanian A 2021 Hubble tension and absolute constraints on the local Hubble parameter *Astron. Astrophys.* **653** A145
[13] Yu H, Ratra B and Wang F-Y 2018 Hubble parameter and baryon acoustic oscillation measurement constraints on the Hubble constant, the deviation from the spatially flat ΛCDM model, the deceleration–acceleration transition redshift and spatial curvature *Astrophys. J.* **856** 3
[14] Jimenez J and Loeb A 2002 Constraining cosmological parameters based on relative galaxy ages *Astrophys. J.* **573** 37–42
[15] Borghi N, Moresco M and Cimatti A 2022 Toward a better understanding of cosmic chronometers: a new measurement of H(z) at $z \sim 0.7$ *Astrophys J. Lett.* **928** L4
[16] Tomasetti E *et al* A new measurement of the expansion history of the universe at z = 1.26 with cosmic chronometers in VANDELS (arXiv:2305.16387)
[17] Cuceu A, Farr J, Lemos P and Font-Ribera A 2019 Baryon acoustic oscillations and the Hubble constant: past, present and future *J Cosmol. Astropart. Phys.* **10** 044
[18] Lindley D 1987 Can the universe be closed? *Nature* **328** 289
[19] PAdam R *et al* (Planck Collaboration) 2016 Planck 2015 results VIII. High frequency instrument data processing: calibration and maps *Astron. Astrophys* **594** A8
[20] Aghanim N *et al* (Planck Collaboration) 2020 Planck 2018 results. V. CMB power *Astron. Astrophys.* **641** A5
[21] Di Valentino E, Melchiorri A and Silk J 2020 Planck evidence for a closed universe and a possible crisis for cosmology *Nat. Astron.* **4** 196–203
[22] Monjo R 2018 Geometric interpretation of the dark energy from projectedhyperconical universes *Phys. Rev.* D **98** 043508
[23] Monjo R and Campoamor-Stursberg R 2020 Lagrangian density and local symmetries of inhomogeneous hyperconical universes *Class. Quantum Grav.* **37** 205015
[24] Bekenstein J D 2004 Relativistic gravitation theory for the modified Newtonian dynamics paradigm *Phys. Rev.* D **70** 083509
[25] Chae K H Lelli F, Desmond H, McGaugh S S, Li P and Schombert J M 2020 Testing the strong equivalence principle: detection of the external field effect in rotationally supported galaxies *Astrophys. J.* **904** 51
[26] Asgari M *et al* 2021 KiDS-1000 cosmology: cosmic shear constraints and comparison between two point statistics *Astron. Astrophys.* **645** A104
[27] Meneghetti M *et al* 2020 An excess of small-scale gravitational lenses observed in galaxy clusters *Science* **369** 6509
[28] Liddle A R 2004 How many cosmological parameters *Mon. Not. Roy. Astron. Soc.* **351** L49–L53
[29] Benisty D and Staicova D 2021 Testing late-time cosmic acceleration with uncorrelated baryon acoustic oscillation dataset *Astron. Atrophys.* **647** A38
[30] Favale A, Gómez-Valent A and Migliaccio M 2023 Cosmic chronometers to calibrate the ladders and measure the curvature of the Universe. A model-independent study *Mon. Not. Roy. Astron. Soc.* **2023** stad1621
[31] Freedman W L *et al* 2019 The Carnegie-Chicago Hubble program. VIII. An independent determination of the Hubble constant based on the tip of the red giant branch *Astrophys. J.* **882** 34
[32] Jimenez R, Cimatti A, Verde L, Moresco M and Wandelt B 2019 The local and distant universe: stellar ages and H0 *J. Cosmol. Astropart. Phys.* **2019** 043

[33] O'Malley E M, Gilligan C and Chaboyer B 2017 Ages and distances of 22 GCs using monte carlo main-sequence fitting *Astrophys. J.* **838** 162
[34] Schlaufman K C, Thompson I B and Casey A R 2018 An ultra Metal-poor star near the hydrogen-burning limit *Astrophys. J.* **867** 98
[35] Kovács A, Beck R, Szapudi I, Csabai I, Rácz G and Dobos L 2020 A common explanation of the Hubble tension and anomalous cold spots in the CMB *Mon. Not. Roy. Astron. Soc.* **499** 320–33
[36] Perlmutter S *et al* 1999 Measurements of Ω and Λ from 42 high-redshift supernovae *Astrophys. J.* **517** 565
[37] Riess A G *et al* 2018 *Astrophys. J.* **853** 126
[38] Riess A G *et al* 2018 New parallaxes of galactic cepheids from spatially scanning the Hubble space telescope: implications for the Hubble constant *Astrophys. J.* **855** 136
[39] Scolnic D M *et al* 2018 The complete light-curve sample of spectroscopically confirmed SNe Ia from Pan-STARRS1 and cosmological constraints from the combined pantheon sample *Astrophys. J.* **859** 101
[40] Zhao D, Zhou Y and Chang Z 2019 Anisotropy of the universe via the Pantheon supernovae sample revisited *Mon. Not. Roy. Astron. Soc.* **486** 5679–89
[41] Cao S, Ryan J and Ratra B 2021 Pantheon and DES supernova, baryon acoustic oscillation and Hubble parameter data to constrain the Hubble constant, dark energy dynamics and spatial curvature *Mon. Not. Roy. Astron. Soc.* **504** 300–10
[42] Font-Ribera A *et al* 2014 Quasar-Lyman α forest cross-correlation from BOSS DR11: baryon acoustic oscillations *J. Cosmol. Astropart. Phys.* **2014** 027
[43] Delubac T *et al* 2015 Baryon acoustic oscillations in the Lyα forest of BOSS DR11 quasars *Astron. Astrophys* **574** A59
[44] Zhang C, Zhang H, Yuan S, Liu S, Zhang T J and Sun Y C 2014 Four new observational H(z) data from luminous red galaxies in the sloan digital sky survey data release seven *Res. Astron. Astrophys.* **14** 1221–33
[45] Jimenez R, Verde L, Treu T and Stern D 2003 Constraints on the equation of state of dark energy and the Hubble constant from stellar ages and the CMB *Astrophys. J.* **593** 622–9
[46] Simon J, Verde L and Jimenez R 2005 Constraints on the redshift dependence of the dark energy potential *Phys. Rev.* D **71** 123001
[47] Moresco M, Verde L, Pozzetti L, Jimenez R and Cimatti A 2012 New constraints on cosmological parameters and neutrino properties using the expansion rate of the Universe to $z \sim 1.75$ *J. Cosmol. Astropart. Phys.* **2012** 053
[48] Gaztañaga E, Cabré A and Hui L 2009 Clustering of luminous red galaxies—IV. Baryon acoustic peak in the line-of-sight direction and a direct measurement of H(z) *Mon. Not. R. Astron. Soc.* **399** 1663–80
[49] Xu X, Cuesta A J, Padmanabhan N, Eisenstein D J McBride C K 2013 Measuring DA and H at z = 0.35 from the SDSS DR7 LRGs using baryon acoustic oscillations *Mon. Not. R. Astron. Soc.* **431** 2834–60
[50] Moresco M *et al* 2016 A 6% measurement of the Hubble parameter at $z \sim 0.45$: direct evidence of the epoch of cosmic re-acceleration *J. Cosmol. Astropart. Phys.* **5** 014
[51] Blake C *et al* 2012 The wigglez dark energy survey: joint measurements of the expansion and growth history at $z < 1$ *Mon. Not. R. Astron. Soc.* **425** 405–14
[52] Ratsimbazafy A L *et al* 2017 Age-dating luminous red galaxies observed with the southern african large telescope *Mon. Not. R. Astron. Soc.* **467** 3239–54
[53] Stern D, Jimenez R, Verde L, Kamionkowski M and Stanford S A 2010 Cosmic chronometers: constraining the equation of state of dark energy. I: H(z) measurements *J. Cosmol. Astropart. Phys.* **2010** 8
[54] Samushia L *et al* 2013 The clustering of galaxies in the SDSS-III DR9 baryon oscillation spectroscopic survey: testing deviations from Λ and general relativity using anisotropic clustering of galaxies *Mon. Not. R. Astron. Soc.* **429** 1514–28
[55] Jiao K, Borghi N, Moresco M and Zhang T-J 2023 New observational H(z) data from full-spectrum fitting of cosmic chronometers in the lEGA-C Survey *Astrophys. J. Supl.* **265** 48
[56] Moresco M 2015 Raising the bar: new constraints on the Hubble parameter with cosmic chronometers at $z \sim 2$ *Mon. Not. R. Astron. Soc. Lett.* **450** L16–L20

[57] Pavsic M and Tapia V 2000 Resource letter on geometrical results for embeddings and branes (arXiv:gr-qc/0010045)
[58] Paston S A and Sheykin A A 2012 Embeddings for the schwarzschild metric: classification and new results *Class. Quantum Grav.* **29** 095022
[59] Bonning E, Marronetti P, Neilsen D and Matzner R 2003 Physics and initial data for multiple black hole spacetimes *Phys. Rev.* D **68** 044019